Geouhys. J. R. astr. Soc. (1971) **23**, 499–530.

Design of a Marine Seismic Reflection Profiling System using Air Guns as a Sound Source

Anton Ziolkowski

(Received 1971 April 23)

Summary

It is normally assumed that all the known information about the source wavelet of a seismic trace is contained in the autocorrelation function of the trace. In such a case it is shown that present marine seismic reflection profiling systems must use minimum-delay source wavelets in order to construct Wiener spiking filters from the autocorrelation function. For the source wavelet to be minimum-delay severe constraints must normally be put on the system; in particular, bubble oscillations must always be suppressed in some way, and thus energy is lost. The method proposed here for the design of Wiener spiking filters to aid the deconvolution of seismic traces, formed using air guns as a sound source, demands only that the pressure, volume and depth of each independent air gun and the depth of the streamer be known. This allows all the available energy to be used. The resulting source waveform, as calculated using the theory of Ziolkowski, though not minimum-delay, can be used in the construction of an efficient Wiener spiking filter.

1. Introduction

The object of a marine seismic reflection survey is to produce clear profiles of the sub-bottom structure immediately beneath the path of the ship. The appearance of the desired profiles is often marred by the presence of noise, and by reverberation or multiple reflections. If the source signal is not a sharp spike but a long oscillating wave train, then every primary and every multiple reflection will also be a long oscillating wave train. In order to produce the desired profiles various processing and instrumental design techniques are employed.

The noise level is often reduced in two ways. One way is to design the detector so that the noise generated by towing it through the water is minimized. The detector array usually consists of a large number of transducers. If the signal correlates from transducer to transducer and the noise does not, the signal to noise ratio from the sum of the responses of each transducer is better than from a single transducer.

The problem of reducing the significance of multiples is often treated by stacking. If a large number of sections of hydrophone streamer are towed behind the survey ship, reflections over the same point can be obtained with consecutive shots, but with varying geometry. When the reflections for each common reflection point are added together, allowing for the geometrical changes, only the ' primary ' reflections correlate and are enhanced. Multiples do not correlate and just contribute to the background noise.

Downloaded from http://gji.oxfordjournals.org/ at Edinburgh University on August 26, 2013

The last problem is to increase the resolution of the reflections by somehow contracting the source wave. If the Earth consisted of layers of perfectly elastic isotropic media any wave would propagate through the Earth without changing its shape. Thus if the source wave were a sharp impulse the seismic trace would consist of a series of sharp impulses, corresponding to the primary reflections and multiples, plus some background noise. However, the Earth does not consist of such ideal layers; absorption of various frequencies takes place in each of the media through which the source wave is transmitted. Thus, even if the source wave were an impulse, the seismic trace would consist of an elaborate series of wavelets, each one arriving at the same time as the corresponding impulse of the ideal trace. Usually the shape of the source wave is more complicated than a simple impulse; the resulting seismogram, therefore, is even more complex. In order to process a seismic trace with a view to contracting each individual wavelet into an impulse, the trace is filtered with a low-pass anti-alias filter and digitized at a sufficiently frequent interval for all the pertinent information to be preserved. The contraction of the source wavelet is then usually performed with a digital Wiener filter (named after Norbert Wiener, 1949).

A Wiener filter is designed with the object of minimizing the root mean square (r.m.s.) difference between the desired digital output and the actual digital output of the filter, for a known digital input. The filter coefficients, f_n, which are separated by the same time interval as the sampled input seismic trace coefficients, are calculated by solving the following set of equations, where x_t is the known real-valued input, and z_t is the desired real-valued output:

$$\sum_{n=0}^{M} f_n \phi_{xx}(n-\tau) = \phi_{zx}(\tau) \quad \text{for} \quad \tau = 0, 1, \ldots, M. \tag{1}$$

In these equations the autocorrelation function is defined as:

$$\phi_{xx}(\tau) = \sum_{t=-\infty}^{\infty} x_{t+\tau} x_t \tag{2}$$

and the cross-correlation function is defined as:

$$\phi_{zx}(\tau) = \sum_{t=-\infty}^{\infty} z_{t+\tau} x_t. \tag{3}$$

The derivation of equations (1) and a fast procedure for their solution is given by Levinson (1949).

Robinson & Treitel (1967) show how equations (1) may be used for source wavelet contraction using the following model for the composition of the seismic trace. The trace, x_t, is assumed to be an additive mixture of signal, u_t, and noise, v_t. Thus:

$$x_t = u_t + v_t.$$

The signal u_t can be considered to be the ideal impulse response of the layered earth, α_t, convolved with an information wavelet, a_t. Thus

$$u_t = \alpha_t * a_t,$$

where the asterisk $*$ denotes convolution. The response, α_t, is a series of knife-sharp impulses representing the primary reflections and multiples. The information wavelet, a_t, represents the source wavelet after its shape has been altered by absorption in the various media through which it has been transmitted. Noise on seismic traces is rarely white, but it can be considered to be white noise which has been smoothed. The noise series, v_t, can be represented as:

$$v_t = \beta_t * b_t,$$

Downloaded from http://gji.oxfordjournals.org/ at Edinburgh University on August 26, 2013

where β_t is a white noise series, whose autocorrelation function, $\phi_{\beta\beta}(\tau)$, therefore vanishes for $\tau \neq 0$, and b_t is some smoothing operator. Robinson and Treitel assume that α_t and β_t are uncorrelated.

To design a Wiener filter to operate on the seismic trace, x_t, a desired output of the form

$$z_t = \alpha_t * d_t$$

is assumed. The wavelet d_t is a much sharper wavelet than the original information wavelet, a_t. The Wiener filter is found by solving equations (1). These are impossible to solve as they stand because the right-hand side coefficients, $\phi_{zx}(\tau)$, cannot yet be computed. However, from their model, Robinson and Treitel show that equations (1) can be reduced to the much simpler set of equations:

$$\sum_{n=0}^{M} f_n[\phi_{aa}(0)\,\phi_{aa}(n-\tau)+\phi_{vv}(n-\tau)] = \phi_{aa}(0)\,\phi_{da}(\tau) \quad \text{for} \quad \tau = 0, 1, \ldots, M \qquad (4)$$

where the autocorrelation functions, $\phi_{\alpha\alpha}(\tau)$, $\phi_{aa}(\tau)$, $\phi_{vv}(\tau)$, are defined as in equation (2), and the cross correlation function, $\phi_{da}(\tau)$, is defined as in equation (3). In this last step it has been assumed that $\phi_{\alpha\alpha}(\tau) = 0$, for all $\tau \neq 0$, which is true for the ideal impulse response assumed, as Treitel & Robinson (1966a) have shown. It has also been assumed that u_t and v_t are uncorrelated. This is perhaps the weakest assumption made, since a large proportion of noise on seismic traces appears to be signal-generated. Therefore some correlation between a_t and v_t would be expected, even if α_t and β_t are uncorrelated.

In the absence of noise equations (4) reduce to

$$\sum_{n=0}^{M} f_n\,\phi_{aa}(n-\tau) = \phi_{da}(\tau) \quad \text{for} \quad \tau = 0, 1, 2, \ldots, M. \qquad (5)$$

It can be seen that the Wiener filter, f_n, will perform the least-squares contraction of the wavelet, a_t, to the desired wavelet, d_t. Therefore, for an input, x_t, the filter, f_n, will attempt to contract every wavelet, a_t, encountered, into the much sharper wavelet, d_t. The factor, $\phi_{aa}(0)$, in equations (4) is only a scaling factor and enters all the right-hand side coefficients.

What is the correct shape for d_t? If d_t is desired to be an impulse it could be chosen so that $d_0 = 1$, $d_\tau = 0$, for all $\tau \neq 0$. In this case all the right-hand side coefficients of equation (4) vanish except for the first one, which is $\phi_{aa}(0)$, a_0 where a_0 is the first coefficient of the information wavelet, a_t. Even if a_0 is not known the filter coefficients, f_n, can be found without difficulty, except for a constant scaling factor. However it may not be possible to design a very effective spiking filter with an impulse in this position. Even if the number of filter coefficients, $M+1$, is large, the filter may give only a poor approximation to a spike on encountering a wavelet a_t as input. It is convenient to describe this filtering process in terms of z-transforms in order to find what may affect the effectiveness of the filter.

The z-transform of the sequence, a_n, is defined as:

$$A(z) = \sum_{n=-\infty}^{\infty} a_n z^n. \qquad (6)$$

Thus the wavelet, a_t:

$$\ldots a_{-2}, a_{-1}, a_0, a_1, a_2, \ldots$$

has the z-transform:

$$A(z) = \ldots + a_{-2}z^{-2} + a_{-1}z^{-1} + a_0 + a_1 z + a_2 z^2 + \ldots .$$

The z-transform has several useful properties which are described by Robinson (1967). We shall be concerned with z-transforms as applied to convolution and

Downloaded from http://gji.oxfordjournals.org/ at Edinburgh University on August 26, 2013

cross-correlation. The convolution of the wavelet, a_t, with coefficients

$$\ldots a_{-2}, a_{-1}, a_0, a_1, a_2, \ldots,$$

with the wavelet b_t, with coefficients $\ldots, b_{-2}, b_{-1}, b_0, b_1, b_2, \ldots$, is defined as:

$$c_t = \sum_{s=-\infty}^{\infty} a_t b_{s-t}. \tag{7}$$

In the z-domain this is equivalent to

$$C(z) = A(z) \,.\, B(z).$$

The cross-correlation of the wavelet a_t with the wavelet b_t is defined as

$$\phi_{ab}(\tau) = \sum_{t=-\infty}^{\infty} a_{t+\tau} b_t. \tag{8}$$

If the a's and b's are complex the cross-correlation of a_t with b_t is defined as

$$\phi_{ab}(\tau) = \sum_{t=-\infty}^{\infty} a_{t+\tau} b_t^*$$

where the asterick * denotes complex-conjugate. In the z-domain this corresponds to

$$\Phi_{ab}(z) = A(z) \,.\, B_r(z),$$

where

$$B_r(z) = \ldots b_2^* z^{-2} + b_1^* z^{-1} + b_0^* + b_{-1}^* z + b_{-2}^* z^2 + \ldots.$$

We notice that

$$B_r(z) = B^*(1/z)$$

and therefore

$$\Phi_{ab}(z) = A(z) \,.\, B_r(z) = A(z) \,.\, B^*(\tfrac{1}{2}).$$

In the special case where a_t and b_t are identical we have

$$\Phi_{aa}(z) = A(z) \,.\, A^*(1/z) \tag{9}$$

or, when a_t is real-valued,

$$\Phi_{aa}(z) = A(z) \,.\, A(\tfrac{1}{2}). \tag{10}$$

It is common in seismic reflection to use the concept of minimum-delay following the work of Robinson (1957). A wavelet is defined to be minimum-delay if all the roots of its z-transform have moduli greater than, or equal to, one. Explicitly, a wavelet, a_t with coefficients

$$a_0, a_1, a_2, \ldots, a_M$$

has the z-transform

$$A(z) = a_M \prod_{i=1}^{M} (z - z_i)$$

where $|z_i| \geqslant 1$ for all i if a_t is minimum-delay.* Another definition of a minimum-delay wavelet exists: of all the wavelets with the same autocorrelation function, that with minimum-delay has the maximum partial energy, E_p, where

$$E_p = \sum_{t=0}^{\tau} |a_t|^2, \quad \tau = 0, 1, \ldots, M-1.$$

* See note added in proof.

Downloaded from http://gji.oxfordjournals.org/ at Edinburgh University on August 26, 2013

These two definitions have been shown to be equivalent by Berkhout (1970). We see from equation (9) that the z-transform of the autocorrelation function, $\Phi_{aa}(z)$, of a_t, is

$$\Phi_{aa}(z) = a_M \prod_{i=1}^{M} (z - z_i)\, a_0^* \prod_{i=1}^{M} \left(1 - \frac{1}{z z_i^*}\right).$$

We may write this last equation as

$$z^M \Phi_{aa}(z) = a_0^* a_M \prod_{i=1}^{M} (z - z_i)\left(z - \frac{1}{z_i^*}\right). \tag{11}$$

Let us now refer back to equations (5), where the presence of noise has been ignored. The filter coefficients, f_n have the z-transform

$$F(z) = f_0 + f_1 z + \ldots + f_M z^M.$$

The input wavelet, a_t, with the coefficients, $a_0, a_1, \ldots a_M$, has the z-transform

$$A(z) = a_0 + a_1 z + \ldots + a_M z^M$$

$$= a_M \prod_{i=1}^{M} (z - z_i).$$

The actual output from the filter, o_t, will have the z-transform

$$0(z) = F(z)\,.\,A(z).$$

If the desired output, d_t, is chosen to be a spike of amplitude one at coefficient d_0, and zero elsewhere, the z-transform of d_t is

$$D(z) = 1,$$

which is minimum-delay. Thus $0(z)$ must have all its energy concentrated very near the front and therefore be, at least approximately, minimum-delay. But, by definition, $0(z)$ can only be minimum-delay if both $F(z)$ and $A(z)$ are minimum-delay. However, because $0(z)$ is only a least-squares approximation to $D(z)$, a better approximation might be achieved by introducing a delay into the desired output, so that $d_m = 1$ and $d_\tau = 0$, for all $\tau \neq m$ (Treitel & Robinson, 1966*b*). The z-transform of d_t now becomes

$$D(z) = z^m,$$

which is not minimum-delay because it has m roots at zero.

It is, in this case, necessary to calculate the first $m+1$ coefficients on the right-hand side of equations (5). These are, apart from a scale factor, $a_m, a_{m-1}, \ldots, a_0$. If a_t is minimum-delay it is possible to construct a_t knowing only $\phi_{aa}(\tau)$. By inspection of equation (11) the z-transform $z^M.\Phi_{aa}(z)$ has $2M$ roots, M of which must satisfy the condition $z_i \geqslant 1$, for $i = 1, 2, \ldots, M$. These ones will form the minimum-delay z-transform of a_t.

But suppose a_t is not minimum-delay. $A(z)$ will then contain one or more roots which lie inside the unit circle (i.e. $|z_i| < 1$ for these roots). Therefore, even if $F(z)$ is minimum-delay $0(z)$ cannot be minimum-delay. In this case the optimum spike position will certainly not be such that $d_0 = 1$, and $d_\tau = 0$, for all $\tau \neq 0$. There will certainly be an optimum delay, m, and the $m+1$ coefficients $a_0, a_1, \ldots, a_m$ must be found to calculate the Wiener filter. By inspection of equation (11) we see that there are 2^M possible choices for an $M+1$-length wavelet, a_t, with this autocorrelation function. This number is reduced if a_t is real valued, for then the roots, if complex, must occur in complex-conjugate pairs. However, unless we know which of the roots of $A(z)$ lie outside the unit circle and which inside, it is a hopeless task to try and find the correct wavelet.

Downloaded from http://gji.oxfordjournals.org/ at Edinburgh University on August 26, 2013

This clearly puts come restriction on the seismic reflection system. If it is assumed that the only knowledge one has of the information wavelet, a_t, is its autocorrelation function $\phi_{aa}(\tau)$, then it is impossible to contract this to a sharp impulse if a_t is not minimum-delay. If some blurring is acceptable, it is possible to suggest that d_t is an abbreviated form of a_t, when the correct Wiener filter can be obtained using the prediction error technique of Peacock & Treitel (1968).

Blurred profiles in general are not acceptable and so a great effort is usually made to constrain the waveforms to be minimum-delay at the source. It has been shown by Berkhout (1970), for example, and we shall show here, that air gun waveforms are not minimum-delay. This is because the waveform is not a simple impulse followed by a uniform decay, but results from the oscillations of a gas bubble in water. The water and air are elastic and there is a periodic exchange of energy between them. The same sort of non-minimum-delay waveform results from the oscillations of an explosive gas bubble. The oscillations or so-called 'bubble pulse' are a problem and have to be reduced in various ways.

Air guns of various sizes are normally used together. The period of oscillation of the bubble produced by each gun differs according to size, depth and internal pressure. By adding guns in the right mixture Giles (1968) has shown how the oscillations cancel, whereas the first impulse adds, if all the guns are fired simultaneously and at the same depth.

The Flexotir system (Lavergne 1968) uses a perforated sphere in which the source explosive charge is detonated. The sphere diameter and perforation size can be determined from Knudsen's theory (1961). The holes in the sphere constrain the water to become turbulent and energy is lost through viscous dissipation, thus reducing the oscillation of the bubble.

The original method of producing an impulsive source with an explosive in water was to detonate it just below the surface. The bubble thus created burst through the surface blowing a plume of water about 200 feet into the air for a 50 lb charge.

All these methods of producing approximately minimum-delay signals sacrifice vast quantities of energy. This is strikingly evident in the case of the water plume. The following design method for a reflection profiling system using air-guns does not use a minimum-delay signal. The z-transform, $A(z)$, of the information wavelet, a_t, is computed with the help of the theory of the oscillation of the bubble produced from an air gun (Ziolkowski 1970).

2. Test of the predictive theory

The method for predicting the output pressure waveform from an air gun described by Ziolkowski (1970), requires that certain parameters concerning the gun be known. In the case shown in Fig. 1 the gun is about to fire and it is desired to predict the pressure waveform which would be measured by a detector hydrophone in the position shown. If the gun volume, V, the depth of the gun below the sea surface, H, and the gauge pressure of the air in the gun at the instant of firing, X, are known, then the pressure wave incident at any point in the water can be predicted. If the sea surface is the only reflector of interest, and the water is sufficiently deep that reflections from the sea floor arrive too late to interfere with the measurable waveform from the gun, then the detector hydrophone will experience two pressure waves: a direct wave from the gun which has travelled a distance D_1; and a reflected wave, which has travelled a distance D_2 and which appears to come from a mirror image of the gun in the sea surface. The mirror image gun appears to behave exactly in antiphase to the real gun because sound waves travelling in water towards the surface suffer a phase change of almost π, as the reflection coefficient is very nearly -1 at the water-air interface. Clearly the amplitudes and relative phases of the two received waves at the detector hydrophone depend on D_1 and D_2.

Downloaded from http://gji.oxfordjournals.org/ at Edinburgh University on August 26, 2013

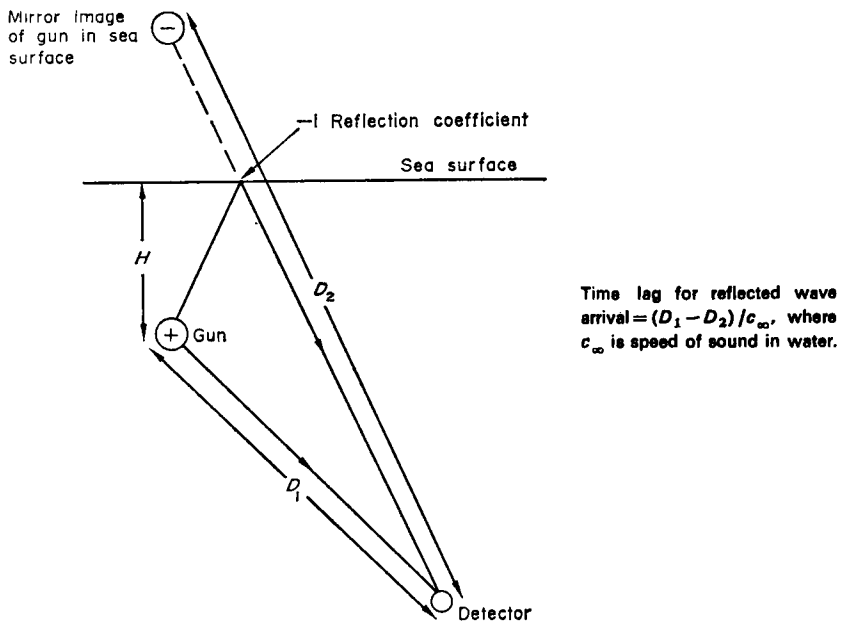


FIG. 1. Diagram to show superposition of direct and reflected pressure waves at a detector.

The pressure wave emitted by the gun is presumed to be derived from a spherical air bubble which initially has the same volume and internal pressure as the air in the gun. It is found that the bulk of the radiation emitted by air guns is of such low frequency that the sizes of the bubbles they produce are small compared with the wavelengths of the radiation. In this case the radiation is independent of the shape of the bubble and therefore only a spherical bubble of the correct volume and internal pressure, and at the same hydrostatic pressure, need be considered.

A measurement of the waveform from a gun in deep water (3000 m) was made, where the following data were applicable: $V = 0{\cdot}155l$ (9·4 cu. in.); $X = 13{\cdot}3\ \mathrm{MNm}^{-2}$ (1940 p. si. g.); $H = 14$ m (46 ft); $D_1 = 6$m (20 ft); $D_2 = 34$ m (112 ft). The bubble oscillation, the predicted detector waveform and the measured waveform are shown in Fig. 2. Apart from the two sharp spikes the appearance of the theoretical wave is very similar to that of the measured wave. The second, smaller spike is due to the later arrival of the reflected wave which has had further to travel and therefore has a smaller amplitude, due to spherical divergence. The initial spike is a result of the initial conditions at the bubble wall.

If the frequency content of the theoretical wave is examined (Fig. 3). it can be seen that significant energy extends up to 500 Hz. It consists of an apparently exponential fall-off with increasing frequency, with superimposed peaks at the fundamental and harmonics of the bubble oscillation frequency. The high frequency content is entirely due to the spikes. In practice the measured waveform cannot have such high frequencies. Even if they exist they would be filtered by the recording electronics and the galvanometer. Normally the frequency content of the source signal is known. The autocorrelation function of the source signal can be found as described in Section 1 and can be separated from the noise spectrum by the method

Downloaded from http://gji.oxfordjournals.org/ at Edinburgh University on August 26, 2013

shown in the Appendix. The power spectrum or intensity spectrum of the signal is the Fourier transform of the autocorrelation function

$$\Phi(f) = \int_{-\infty}^{\infty} \phi(\tau) \exp(-2\pi i f\tau)\, d\tau.$$

It is reasonable, therefore, to filter the theoretical signal with a low-pass filter to remove the high-frequency content. This has been done with the theoretical waveform of Fig. 3. The filter used was a Gaussian filter, $\exp(-\alpha f^2)$, where α was chosen so that the attenuation was $\exp(-1)$ at a frequency, f, of 300 Hz. The result of filtering this wave can be seen in Fig. 4, where the theoretical and measured waveforms are compared.

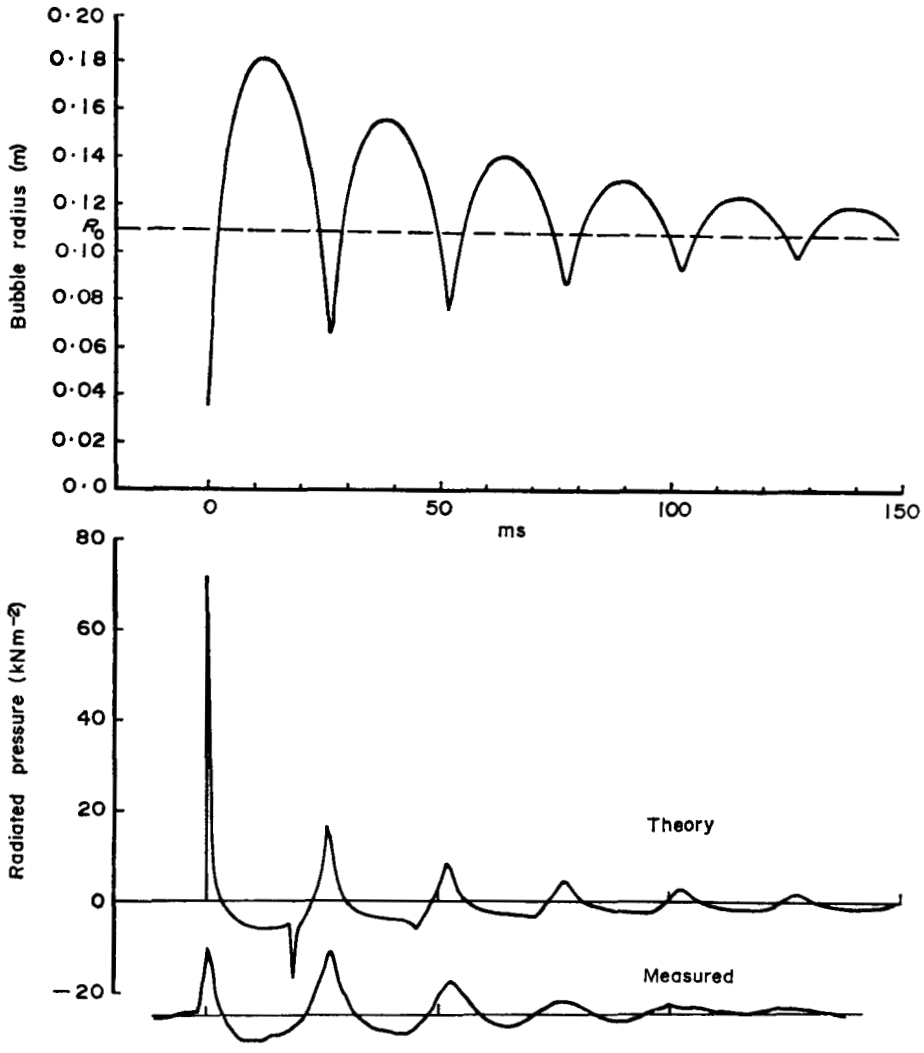


FIG. 2. Comparison of theoretical and measured waveforms for a gun for which $V = 0{\cdot}1551$, $X = 13{\cdot}3$ MNm^{-2}, $H = 14$ m, $D_1 = 6$ m, $D_2 = 34$ m. R_0 is the bubble radius at which the internal pressure and hydrostatic pressure are equal.

Downloaded from http://gji.oxfordjournals.org/ at Edinburgh University on August 26, 2013

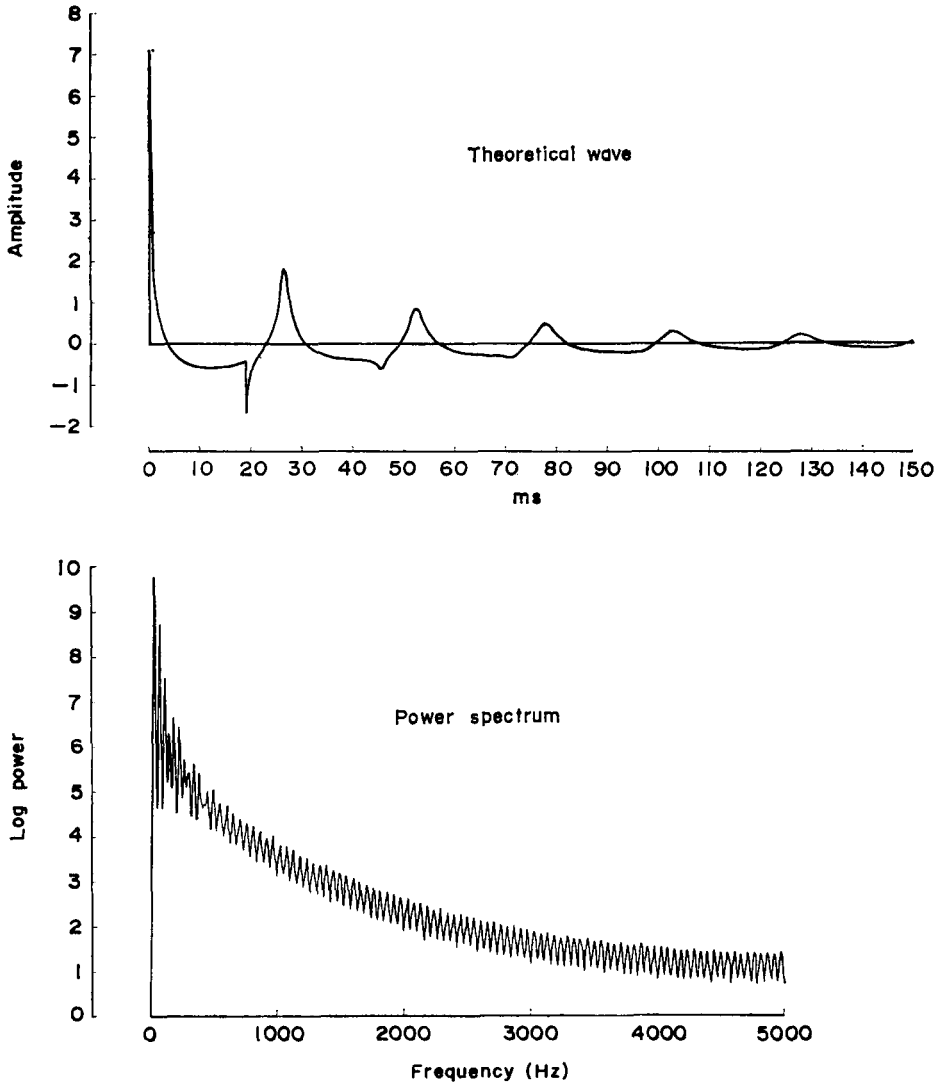


FIG. 3. The theoretical wave of Fig. 2 and its power spectrum. The amplitudes have been scaled arbitrarily.

The theoretical and measured waveforms are now seen to be in very close agreement. It can be seen that sampling both waveforms at 2 ms intervals, giving a Nyquist frequency of 250 Hz, will introduce a small amount of aliasing—when energy at frequencies above the Nyquist frequency appears at frequencies below the Nyquist—which, as shall be shown later, is not intolerable and even desirable, if not necessary.

It is now possible to test this predictive method for Wiener filtering. The Wiener filter coefficients, $f_0, f_1, \ldots, f_M$, are calculated from equations (5), where the wavelet $a_0, a_1, \ldots, a_M$ is the sampled theoretical waveform of Fig. 4, and the desired output is d_τ, where $d_n = 1$, and $d_\tau = 0$ for all $\tau \neq n$. The integer n is varied until the optimum filter has been found. Some criterion must be used to define the meaning of an 'optimum filter'. Levinson (1949) shows that by increasing the number of filter coefficients the quality of the filter can always be improved; the desired filter output

Downloaded from http://gji.oxfordjournals.org/ at Edinburgh University on August 26, 2013

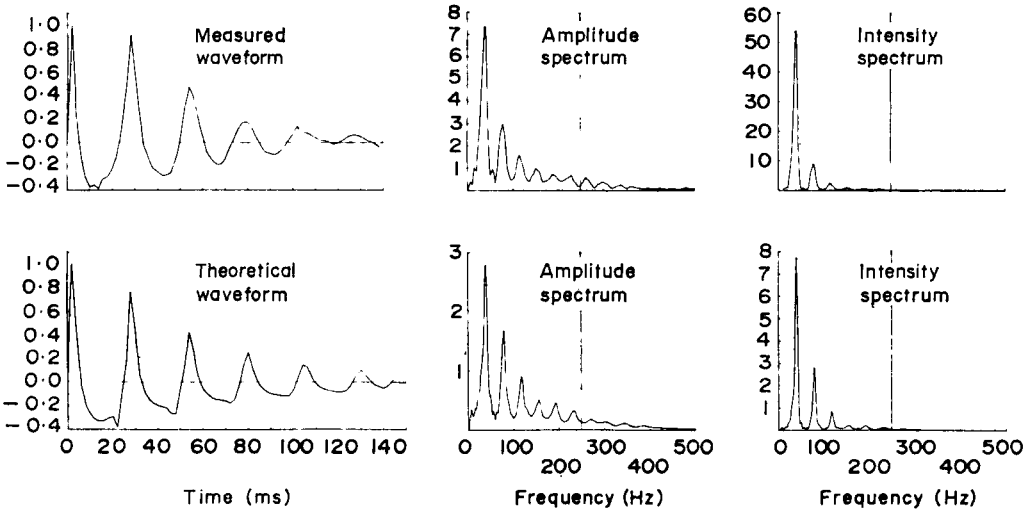


FIG. 4. Comparison of the measured waveform of Fig. 2 and its spectra with the filtered theoretical waveform of Fig. 2 and its spectra. All amplitudes have been scaled arbitrarily.

and the actual filter output resemble each other more and more. The Wiener filter minimizes the r.m.s. difference between the desired output, d_t, and the actual output, o_t, of the filter. Thus the average squared error

$$I = \frac{1}{2t+1} \sum_{t=-\infty}^{\infty} (d_t - 0_t)^2$$

is a minimum. In the case being considered n was varied so that the shortest filter which would reduce I to less than 0·05 was considered to be the 'optimum filter'. The optimum filter, the result of filtering the theoretical wave, and the result of filtering the measured wave are all shown in Fig. 5.

This filter quality was achieved with 34 coefficients. It can be seen that the real wave has been compressed into a spike of very short duration compared with the original length of the wave. Thus, although the amplitude and phase information of the real wave cannot be exactly determined from the calculation described above, a very satisfactory approximation can be achieved which gives excellent results when used for Wiener filtering.

It was shown in Section 1 that the $2M+1$-length z-transform of the autocorrelation function provides information which allows 2^M wavelets of length $M+1$ to be computed, all of which have exactly the same autocorrelation function. However, the autocorrelation function contains no phase information and thus there is no means of knowing which of these 2^M possible wavelets is the right one. The difference between these two techniques lies in the fact that the deterministic method gives both amplitude and phase information, though only approximately.

The position of the spike in Fig. 5 suggests that the waveforms are not minimum-delay. To test whether they are minimum-delay or not it is only necessary to factorize the z-transforms

$$A(z) = a_0 + a_1 z + \ldots + a_M z^M$$

of the real waveform, and

$$A^1(z) = a_0{}^1 + a_1{}^1 z + \ldots + a_M{}^1 z^M$$

Downloaded from http://gji.oxfordjournals.org/ at Edinburgh University on August 26, 2013

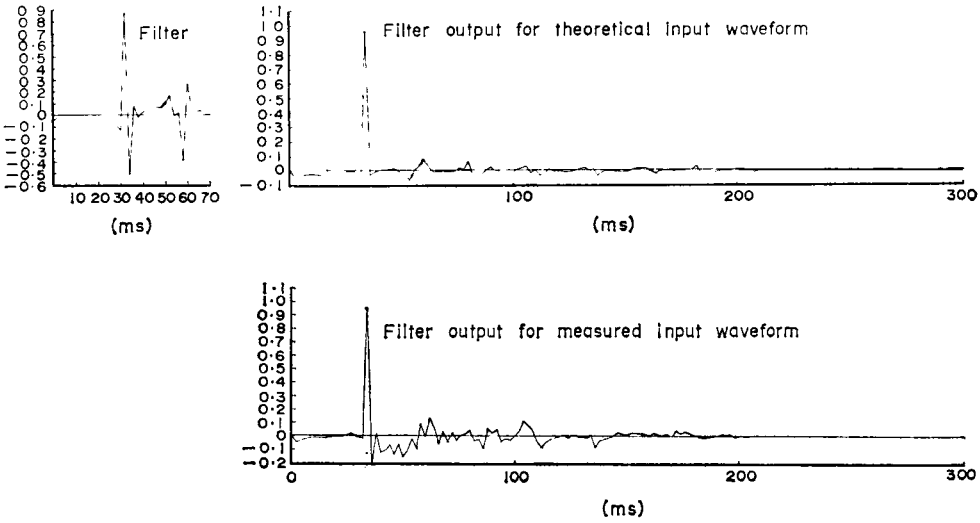


FIG. 5. The spiking filter for the theoretical waveform of Fig. 4, and a comparison of the outputs for the theoretical and measured waveforms of Fig. 4 as inputs.

of the theoretical waveform, and to see whether all the roots lie outside the unit circle. In this case M is 69. The factorisation of polynomials of this degree is not trivial (Bareiss 1968). However, since we do not need to know where all the roots are in the complex plane, but only need to know whether they lie inside the unit circle or not, we may count the number of roots inside the unit circle using Cauchy's Principle of the Argument (Copson 1970).

Cauchy's Principle of the Argument states that if C is a closed loop in the complex plane and if f is a function of a complex variable, z, the number

$$m = \frac{1}{2\pi i} \int_C \frac{f^1(z)}{f(z)}\, dz$$

is equal to the excess of the number of zeros of $f(z)$ within C over the number of poles there. In the present case $f(z)$ is the z-transform of the waveform, which contains no poles, c is the unit circle:

$$z = \exp(i\theta),$$

and therefore m is the number of roots of $f(z)$ lying inside the unit circle. The above integration reduces to

$$m = \frac{1}{2\pi} [\arg(f(z))]_C.$$

Thus the number of complete revolutions of

$$f(z) = |f(z)| \exp(i\phi)$$

as z varies round the unit circle is equal to the number of roots of $f(z)$ inside the unit circle. It is possible that $f(z)$ will vary too fast if θ is not incremented in sufficiently small increments. Therefore a check on the procedure is required.

It was shown in Section 1 that if

$$A(z) = a_0 + a_1 z + \ldots + a_n z^n$$

Downloaded from http://gji.oxfordjournals.org/ at Edinburgh University on August 26, 2013

then the reverse polynomial

$$A_{rev}(z) = a_n^* + a_{n-1} z + \ldots + a_0^* z^n = z^n A^*(1/z).$$

If the coefficients, a_i, $i = 0, 1, \ldots, n$ are real, then

$$A_{rev}(z) = z^n A(1/z).$$

The roots, z_i, $i = 1, 2, \ldots, n$, of $A(z)$ are the reciprocals of the complex conjugates of the roots of $A_{rev}(z)$. That is, the roots of $A_{rev}(z)$ are $(1/z_i^*)$, $i = 1, 2, \ldots, n$. Therefore if the z-transform $A(z)$ has n roots, m of which lie inside the unit circle, the z-transform $A_{rev}(z)$ has $n-m$ roots inside the unit circle. This is not true if $A(z)$ has any roots exactly on the unit circle for then $A_{rev}(z)$ has an equal number of roots also on the unit circle and $A(z)$ and $A^*(1/z)$ both have value zero when z is at these roots. It is thus possible to count all the roots of the z-transform $A(z)$.

The z-transforms $A(z)$ and $A^1(z)$ of the real and theoretical waveforms of Fig. (4) are both of degree 69 and were tested using Cauchy's Principle of the Argument. It was found that, by evaluating $A(z)$, the z-transform of the measured wave, for only 3000 equi-spaced points on the unit circle, four of the 69 roots were missed. When the number of points was increased to 5000 all the roots were found to be either inside or outside the unit circle. The same applied to $A^1(z)$, the z-transform of the theoretical wave: none of the roots lay exactly on the unit circle.

The plots of the functions $A(z)$ and $A^1(z)$ are shown in Figs 6 and 7. The value of ϕ for the argument of $A(z)$ was found to have increased by 10π, whereas the value of ϕ for the argument of $A^1(z)$ was found to have increased by 4π. Thus neither wavelet is minimum-delay. The real wave has five roots inside the unit circle, one of which is real, and 64 outside; the theoretical wave has two roots inside and 67 outside. Two of the roots of $A(z)$ lie very close to the unit circle as can be seen from Fig. 6: the function goes very close to zero on two occasions.

It has thus been conclusively shown that the measured waveform is not minimum-delay, that it could not have been predicted from its autocorrelation function alone, and that the deterministic method described above provides a satisfactory prediction. It will be shown in Sections 3 and 4 of this paper how this method can be used in the design of a seismic reflection profiling system.

3. Application of the method to the design of a system with one air gun

Fig. 8 shows a seismic reflection system with the source at depth H, the hydrophone streamer at depth D, and the bottom of the sea at depth W. Some criterion must be used by which the system response can be optimized. The criterion used here is that the energy in the near-vertical incidence reflected arrival from a perfect horizontal reflector shall be a maximum. This merely means that the source and its mirror image should produce a radiation pattern with the peak energy in the vertical direction, and that the receiver and its mirror image should be most sensitive to this energy returning from vertically below.

The first step in the design of the system is to determine the depth, H, of the source. This can be done by considering the point P on the surface of a perfect reflector at the sea floor. It is assumed that the water depth, W, is very much greater than the source depth, H. In these conditions the direct pressure wave from the source, $PD(t)$, and the reflected wave from the surface $PR(t)$, have the same amplitude but opposite polarity, and $PR(t)$ lags $PD(t)$ by a time t_0, where

$$t_0 = 2H/c_\infty \tag{12}$$

and c_∞ is the speed of sound in water. This is illustrated in Fig. (9). The waveform incident at the point P in Fig. (8) is $PT(t)$ where

$$PT(t) = PR(t) + PD(t).$$

Downloaded from http://gji.oxfordjournals.org/ at Edinburgh University on August 26, 2013

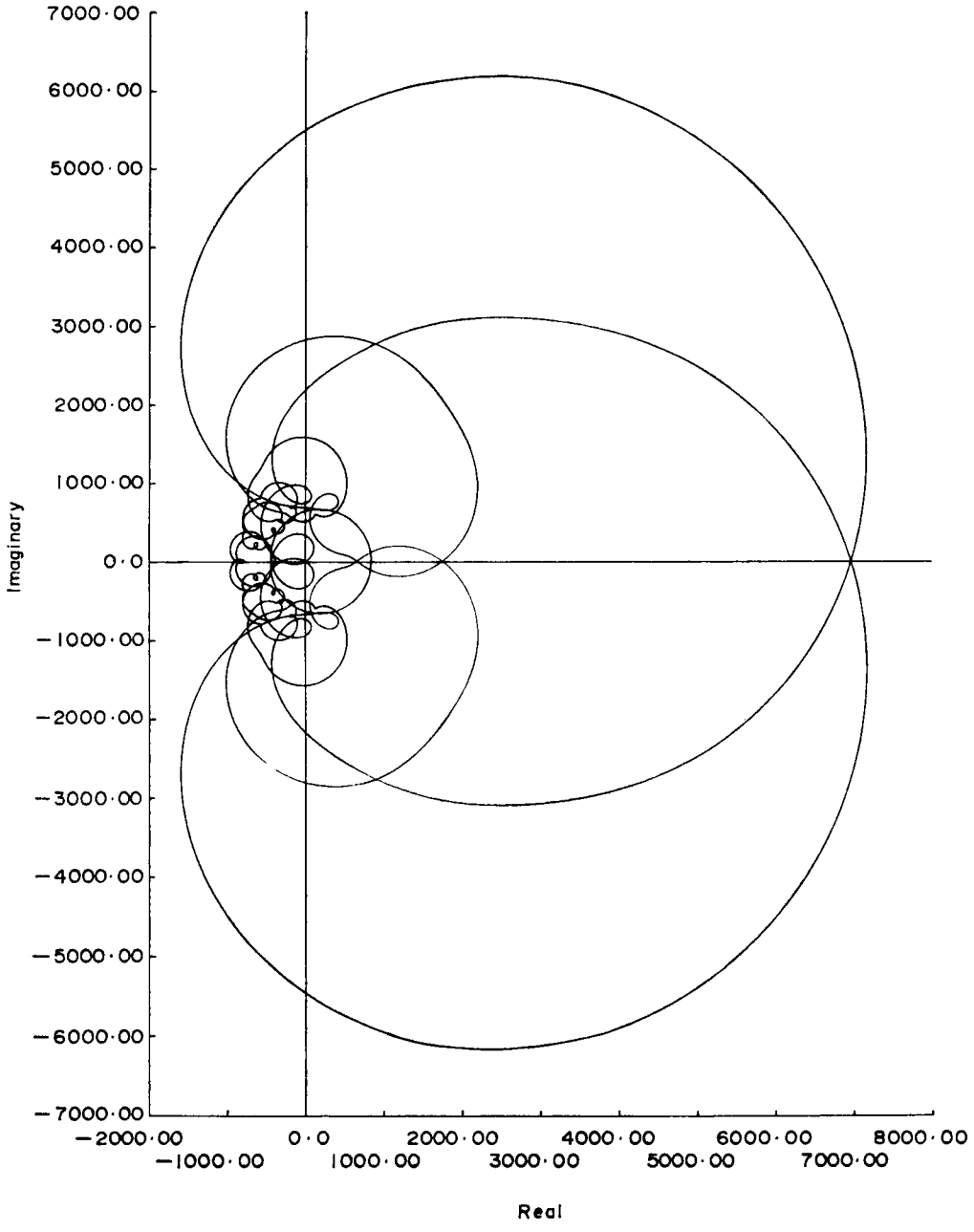


FIG. 6. Variation of the z-transform, $A(z)$, of the measured waveform as z is varied round the unit circle. The observed symmetry is $A^*(z) = A(z^*)$ which is a result of $A(z)$ having real coefficients.

Downloaded from http://gji.oxfordjournals.org/ at Edinburgh University on August 26, 2013

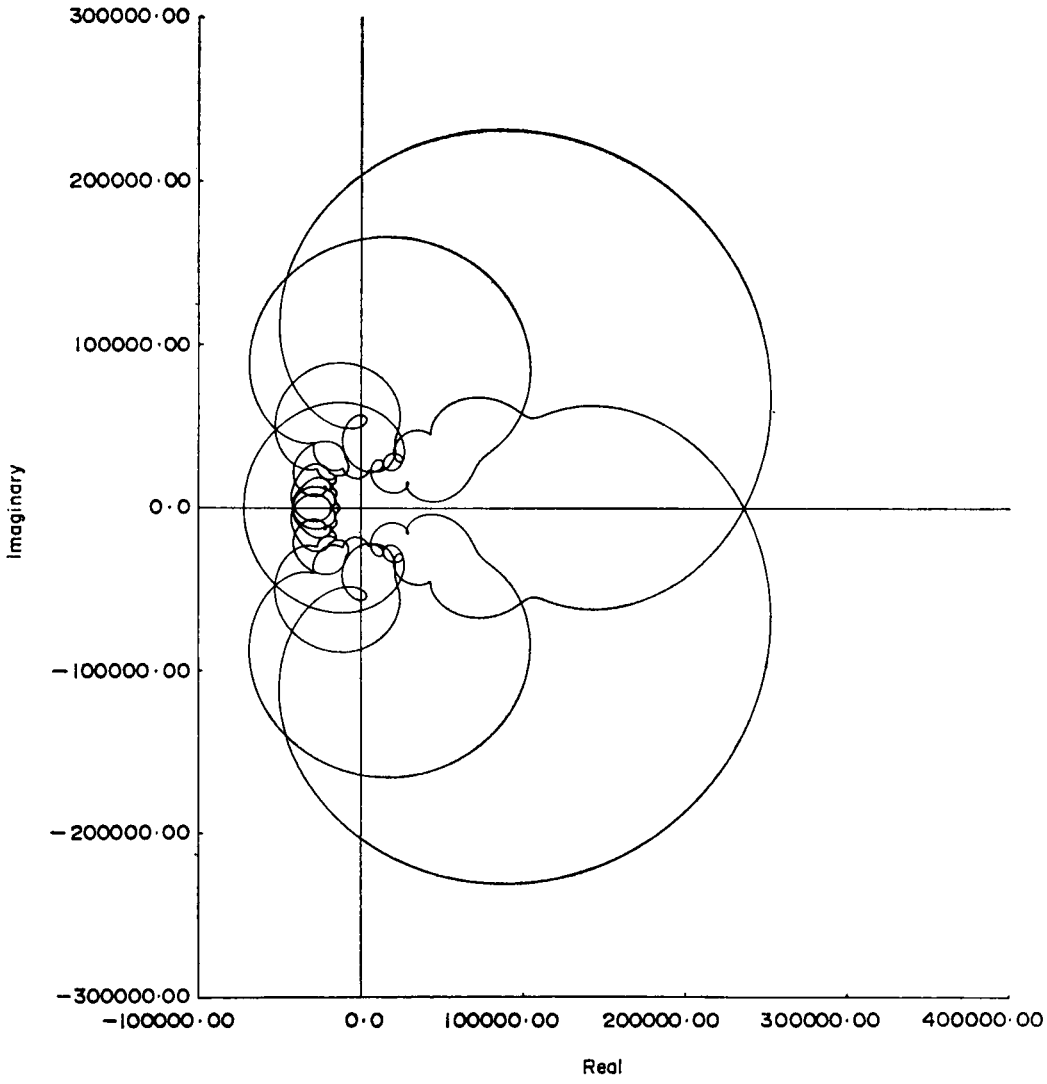


FIG. 7. Variation of the z-transform, $A^1(z)$, of the theoretical waveform as z is varied round the unit circle. The observed symmetry is $A^{1*}(z) = A^1(z^*)$ which is a result of $A^1(z)$ having real coefficients.

Downloaded from http://gji.oxfordjournals.org/ at Edinburgh University on August 26, 2013

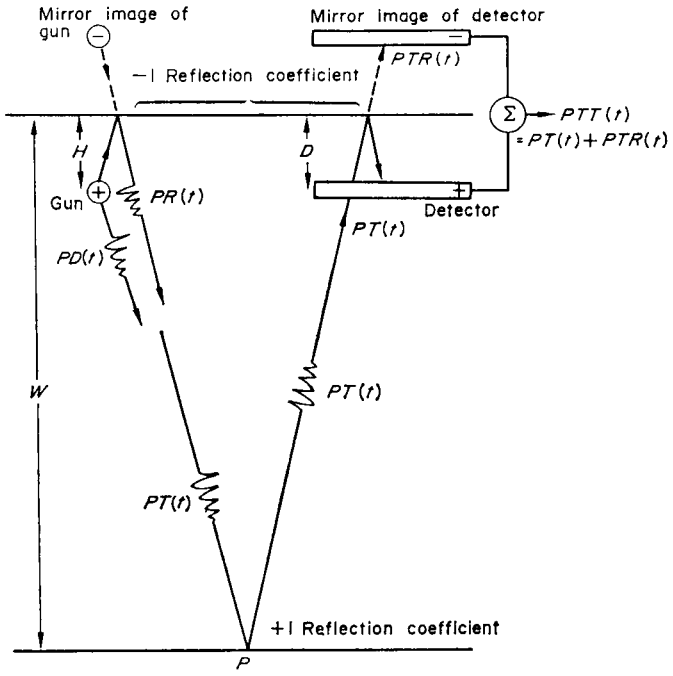


FIG. 8. A diagram of an idealized seismic reflection system showing the surface reflection effect for a perfect reflection at the sea floor.

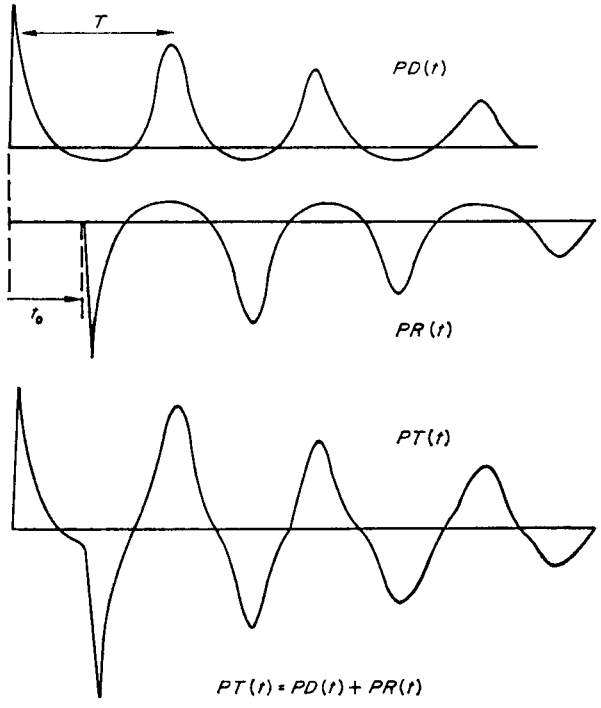


FIG. 9. Superposition of the direct wave and its surface reflection at the point P in Fig. 8. The time lag $t_0 = 2H/c_\infty$, where c_∞ is the speed of sound in water.

Downloaded from http://gji.oxfordjournals.org/ at Edinburgh University on August 26, 2013

It can be seen from a consideration of Fig. (9) that the energy in $PT(t)$ can be a maximum if

$$t_0 = \tfrac{1}{2}T \tag{13}$$

where T is the first period of oscillation. In this case the negative peaks in $PR(t)$ add with the negative peaks in $PD(t)$ and the positive peaks in $PR(t)$ add with the positive peaks in $PD(t)$. Combining equations (12) and (13) to find the optimum depth, H_{0p}, of the source, we find

$$H_{0p} = c_\infty \cdot T/4. \tag{14}$$

However, the first period of oscillation, T, is a function of volume, pressure and depth of the gun; thus

$$T = T(V, X, H)$$

Figs 10–13 show how the first period, T, varies with depth, H, for guns of varying sizes (10–100 cu. in.) at constant pressure. All these curves were obtained using the bubble theory (Ziolkowski 1970) and an assumed equation of state relating the internal pressure, P, in the bubble, to the bubble radius, R:

$$P = p_\infty \left(\frac{R_0}{R}\right)^{3.4}$$

where p_∞ is the hydrostatic pressure, and R_0 is the bubble radius for which $P = p_\infty$. The intersection of the straight line, equation (14), with these curves, gives the optimum depth, H_{0p}, and the bubble oscillation period, T, for each gun size at the given pressure. The variation of optimum depth with pressure for all the different

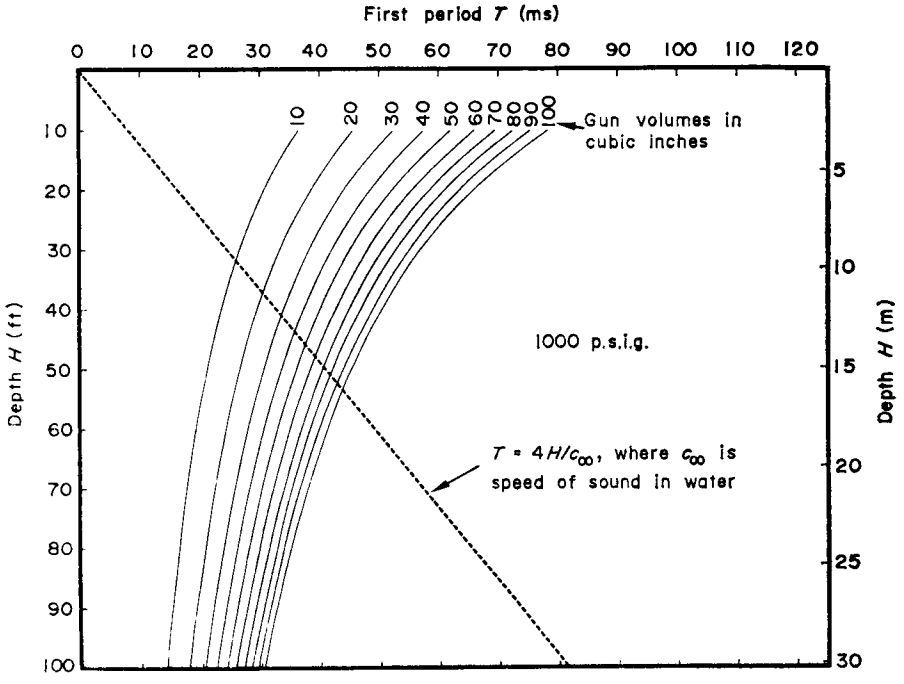


FIG. 10. Variation of the first period of oscillation, T, of the bubble with the depth, H, of the gun, for guns 10–100 cu. in. firing at 1000 p.s.i.g.

Downloaded from http://gji.oxfordjournals.org/ at Edinburgh University on August 26, 2013

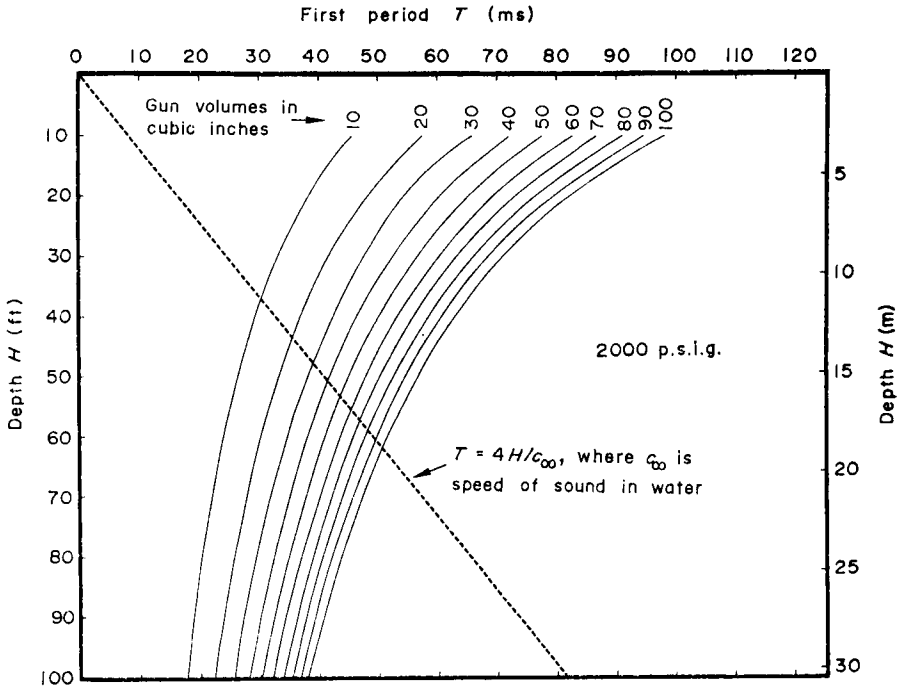


FIG. 11. Variation of the first period of oscillation, T, of the bubble with the depth, H, of the gun, for guns 10–100 cu. in. firing at 2000 p.s.i.g.

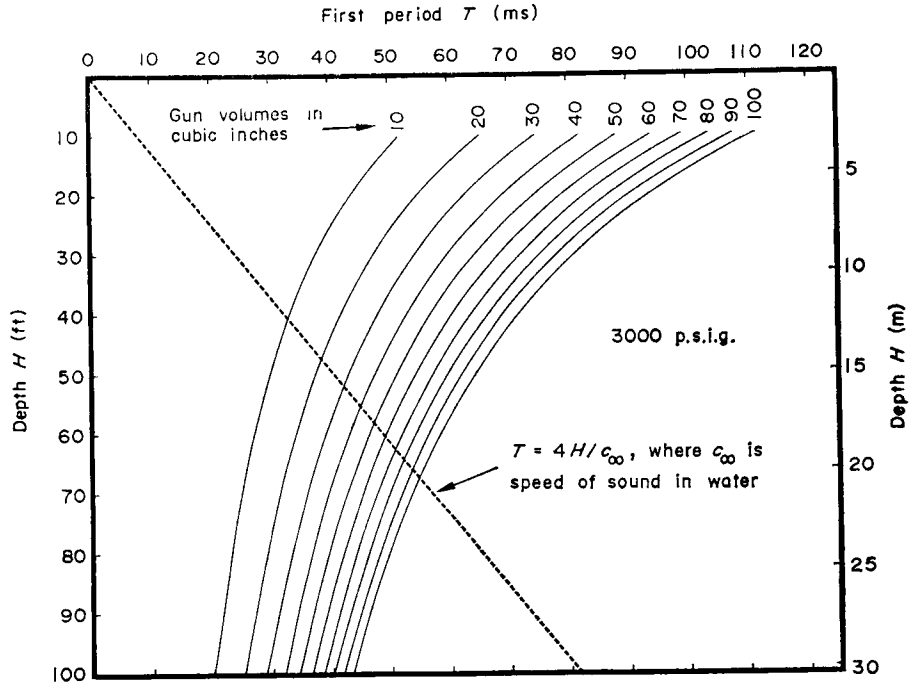


FIG. 12. Variation of the first period of oscillation, T, of the bubble with the depth, H, of the gun, for guns 10–100 cu. in. firing at 3000 p.s.i.g.

Downloaded from http://gji.oxfordjournals.org/ at Edinburgh University on August 26, 2013

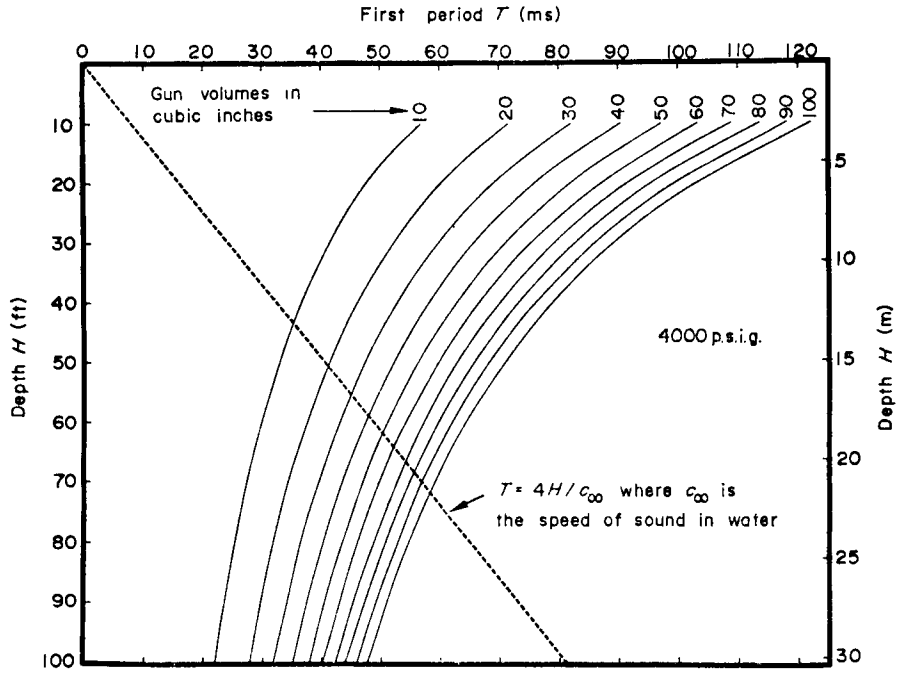


FIG. 13. Variation of first period of oscillation, T, of the bubble with the depth, H, of the gun, for guns 10–100 cu. in. firing at 4000 p.s.i.g.

guns can be found by combining the information in Figs 10–13. This is shown in Fig. 14.

The total response of the receiver, if it is perfectly linear, can be denoted

$$PTT(t) = PT(t) + PTR(t)$$

where $PTR(t)$ is the negative, time-delayed, mirror-image response to the received wave, $PT(t)$. Because the sea floor is assumed here to be a perfect reflector, the received wave $PT(t)$ will be identical with the incident wave at the reflection point, P, on the sea floor, apart from a scale factor of $\frac{1}{2}$, due to spherical divergence. In practice it is possible to calculate $PD(t)$ and $PR(t)$ as if they travel a distance $2W$; this will also allow for the small effect of the variation of amplitude due to the fact that the speed of sound varies with the amplitude of the pressure wave being transmitted (Kirkwood & Bethe 1942). Thus the change of shape of $PT(t)$ which will take place between the point P and the receiver can be taken into account. Since $PTR(t)$ is a negative version of $PT(t)$, delayed by an amount

$$t_1 = 2D/c_\infty \tag{16}$$

it is clear from Fig. 15 that $PT(t)$ and $PTR(t)$ add in phase to make the energy in $PTT(t)$ a maximum when

$$t_1 = \tfrac{1}{2}T. \tag{17}$$

Combining equations (16) and (17) to find the optimum depth, D_{0p}, of the receiver, we have

$$D_{0p} = c_\infty T/4. \tag{18}$$

Downloaded from http://gji.oxfordjournals.org/ at Edinburgh University on August 26, 2013

Therefore the receiver and gun should be at the same depth, $c_\infty T/4$, for a maximum energy response of the system for a near-vertical reflection from a perfect reflector. If the reflection coefficient is not $+1$ at the reflector of interest, the shape of $PT(t)$ is not altered on reflection, but its amplitude is smaller, since some of the incident energy is transmitted. If the angle of incidence is small, the depths H_{0p} and D_{0p}, given by equations (14) and (18) are optimum. The depth $c_\infty T/4$ is equal to $\lambda/4$

$$c_\infty T/4 = \lambda/4,$$

where λ is the wavelength of the bubble oscillation frequency, $1/T = f_0$ in water. This result is not surprising if a transmission lines analogy is considered.

This method of matching the energy response of the system to the bubble oscillation period was used by Cambridge University and the National Institute of Oceanography in 1969, when they discovered a sedimentary basin on Rockall Plateau by means of seismic reflection (Roberts *et al.* 1970).

It is now convenient to test whether it is possible to filter the received waveform, $PTT(t)$, into a spike, and to test the spiking filter on real data. At the time of writing there is only one available record for which the parameters H, V, X, D and W are known. This is shown in Fig. 20(a). The data applicable to this trace are as follows: $H = 14 \pm 1{\cdot}5$ m $(45 \pm 5$ ft); $V = 0{\cdot}51$ $(30{\cdot}5$ cu. in.); $X = 11{\cdot}7 \pm 0{\cdot}3$ MNm^{-2} $(1700 \pm 50$ p.s.i.g.); $D = 15 \pm 1{\cdot}5$ m $(48 \pm 5$ ft); $W =$ about 2300 m (1200 fm). As long as the water depth, W, is large compared with the gun depth, H, and receiver depth, D, the value of W does not need to be known accurately for the determination of the shape of the arrival wave, $PTT(t)$. The main effect of varying W is to alter

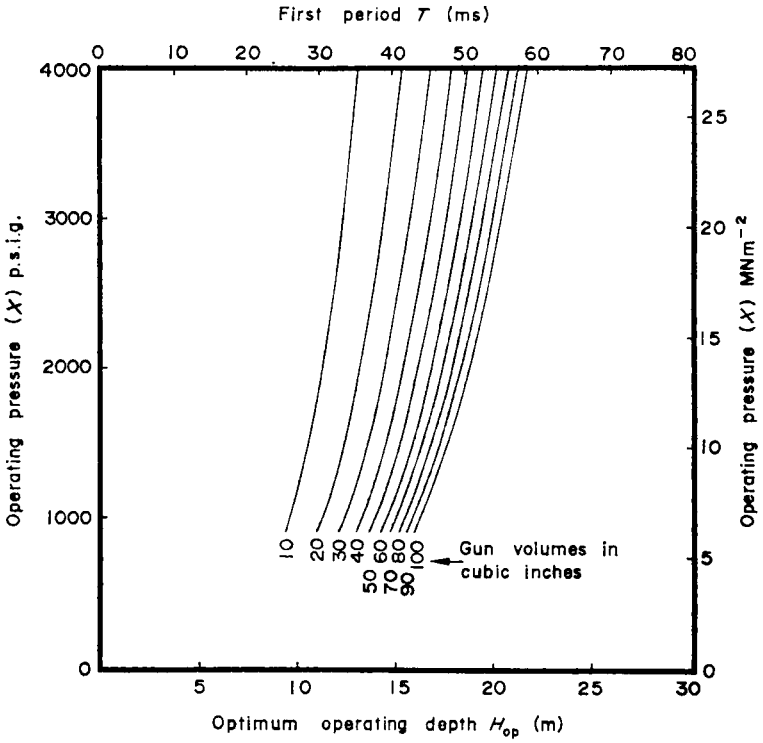


FIG. 14. Variation of the optimum operating depth, H_{op}, and first period of oscillation, T, with the operating pressure of the gun, X, for guns 10–100 cu. in.

Downloaded from http://gji.oxfordjournals.org/ at Edinburgh University on August 26, 2013

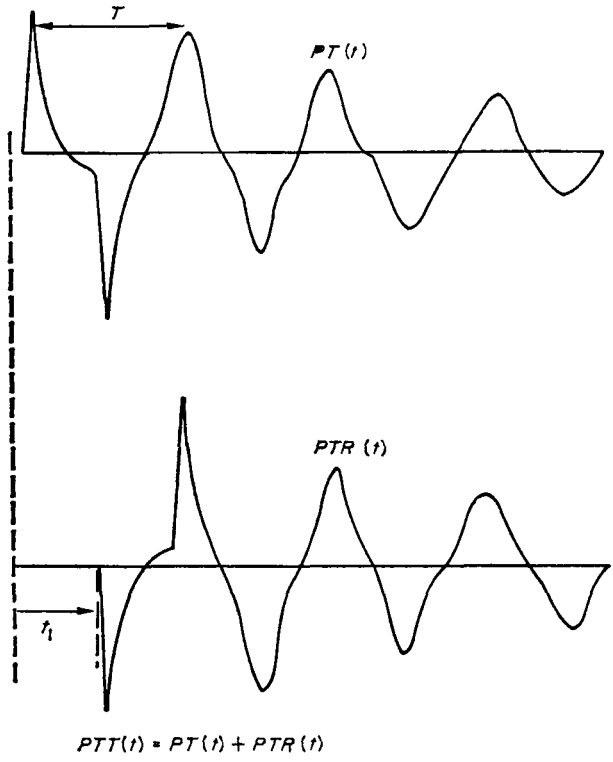


FIG. 15. Superposition of the direct wave and its surface reflection for a reflection from the point P in Fig. 8. The time lag $t_1 = 2D/c_\infty$, where c_∞ is the speed of sound in water.

the amplitude of $PTT(t)$; for large values of W the amplitude of $PTT(t)$ is inversely proportional to W. The seismic trace of Fig. 20(a) was recorded over the very narrow frequency band of 20–40 Hz.

The energy build-up by addition of surface reflections for the available data is shown in Fig. 16. It will be noticed that the first peak of $PTR(t)$ does not quite add in phase with the first negative peak of $PT(t)$. This slight lag of $PTR(t)$ with respect to $PT(t)$ is caused by the slightly greater depth of the receiver than of the source. However, on filtering with a low-pass Gaussian, $\exp(-\alpha f^2)$, filter with a cut-off of $\exp(-1)$ at 50 Hz, small details like this disappear. This can be seen in the last waveform of Fig. 16.

It is now necessary to calculate a spiking filter for the waveform $PTT(t)$, after low-pass filtering, that is, for the last waveform of Fig. 16. This, however, is not immediately possible, as will be seen from the following considerations.

It was shown in Section 1 of this paper that the output, o_t, of a filter, f_n, for an input, x_t, is the convolution of f_n with x_t

$$o_t = f_n * x_t.$$

Convolution of two functions in the time-domain corresponds to multiplication of their Fourier transforms in the frequency-domain. Thus

$$O(\nu) = F(\nu) \,.\, X(\nu). \tag{19}$$

Downloaded from http://gji.oxfordjournals.org/ at Edinburgh University on August 26, 2013

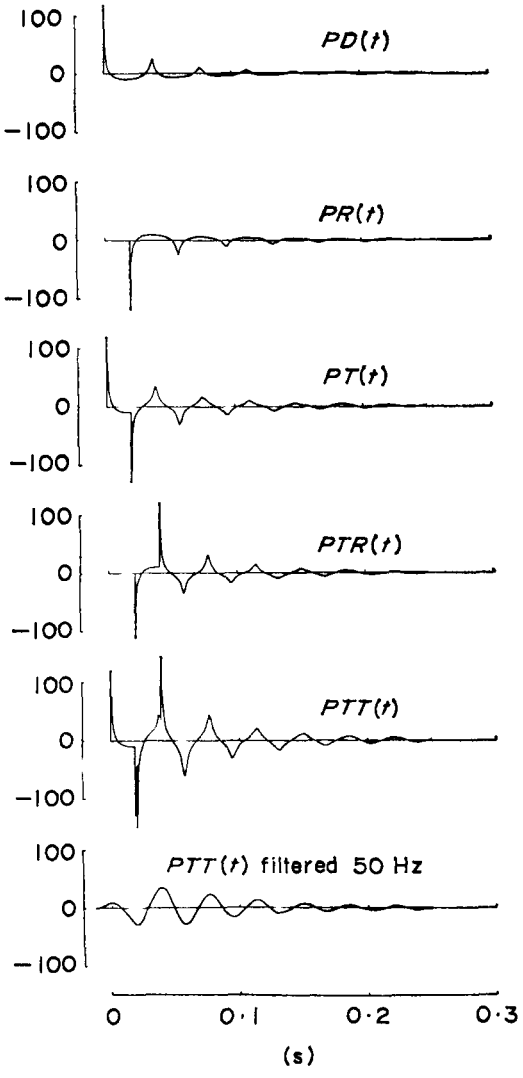


FIG. 16. Energy build-up of surface reflected waves for the system shown in Fig. 8 for which the following data are applicable: $H = 14$ m; $V = 0{\cdot}51$, $X = 11{\cdot}7$ MNm^{-2}, $D = 15$ m, $W = 2300$ m. The last waveform in the result of filtering $PTT(t)$ with a low pass filter of cutoff e^{-1} at 50 Hz. Amplitude scale is in Nm^{-2}.

Downloaded from http://gji.oxfordjournals.org/ at Edinburgh University on August 26, 2013

The Fourier transform, $G(v)$, of a time function, $g(t)$, is defined as

$$G(v) = \int_{-\infty}^{\infty} g(t) \exp(-2\pi i v t)\, dt. \tag{20}$$

The inverse transform, $g(t)$, is defined as

$$g(t) = \int_{-\infty}^{\infty} G(v) \exp(2\pi i v t)\, dv. \tag{21}$$

If $g(t)$ is a discrete time series, g_t, where t only takes integer values, the discrete Fourier transform, G_v, of g_t is defined as

$$G_v = \lim_{N\to\infty} \sum_{t=-N}^{N} g_t \exp[-2\pi i v t/(2N+1)] \tag{22}$$

where

$$g_t = \lim_{N\to\infty} \frac{1}{2N+1} \sum_{v=-N}^{N} G_v \exp[2\pi i v t/(2N+1)]. \tag{23}$$

It can be seen that the discrete Fourier transform, G_v, is a special case of the z-transform,

$$G(z) = \sum_{t=-\infty}^{\infty} g_t z^t \tag{24}$$

when $z = \exp[-2\pi i v/(2N+1)]$. The discrete Fourier transform, G_v, has amplitude, $|G_v|$, and phase, θ_v, at frequency v. Thus it may be written as

$$G_v = \sum_{v=-\infty}^{\infty} |G_v| \exp(i\theta_v).$$

Equation (19) may be written as

$$\sum_{v=-\infty}^{\infty} |O_v| \exp(i\phi_v) = \sum_{v=-\infty}^{\infty} |F_v| \exp(i\psi_v) \,.\, |X_v| \exp(i\theta_v) \tag{25}$$

where ϕ_v, ψ_v and θ_v correspond to the phases of O_v, F_v and X_v at frequency v. Equation (25) may be rearranged to give:

$$\sum_{v=-\infty}^{\infty} |F_v| \exp(i\psi_v) = \frac{\sum_{v=-\infty}^{\infty} |O_v| \exp(i\phi_v)}{\sum_{v=-\infty}^{\infty} |X_v| \exp(i\theta_v)} \tag{26}$$

The filter, f_n, will be unstable whenever $|F_v|$ tends to infinity, which will occur whenever $|X_v|$ tends to zero. The function $|X_v|$ as a function of v is known as the amplitude spectrum of the input trace, x_t. If this contains zeros, the filter will become unstable. In terms of calculating the filter coefficients, the f_n, from a theoretical waveform, a_t, the relevant equations are equations (5)

$$\sum_{n=0}^{M} f_n \phi_{aa}(n-\tau) = \phi_{da}(\tau) \quad \text{for} \quad \tau = 0, 1, \ldots, M. \tag{5}$$

Downloaded from http://gji.oxfordjournals.org/ at Edinburgh University on August 26, 2013

Equation (5) may be written as

$$\begin{bmatrix} \phi_{aa}(0) & \phi_{aa}(1) & \dots & \phi_{aa}(M) \\ \phi_{aa}(-1) & \phi_{aa}(0) & \dots & \phi_{aa}(M-1) \\ \vdots & \vdots & & \vdots \\ \phi_{aa}(-M) & \phi_{aa}(-M+1) & \dots & \phi_{aa}(0) \end{bmatrix} \begin{bmatrix} f_0 \\ f_1 \\ \vdots \\ f_M \end{bmatrix} = \begin{bmatrix} \phi_{da}(0) \\ \phi_{da}(1) \\ \vdots \\ \phi_{da}(M) \end{bmatrix}.$$

Or, more concisely,

$$F \,.\, \Phi_{aa} = \Phi_{da}. \tag{27}$$

Equation (27) may be written as

$$F = \Phi_{aa}^{-1} \,.\, \Phi_{da}. \tag{28}$$

The calculation of the matrix F will go unstable whenever the determinant, $\det \Phi_{aa}$, of the matrix Φ_{aa}, tends towards zero. The matrix equation (28) is analogous to the Fourier transform equation (26), with the filter input, x_t, replaced by the theoretical input, a_t, and the actual filter output, o_t, replaced by the desired filter output, d_t. The Fourier transform of the autocorrelation function of a waveform is the power spectrum of the waveform; the power spectrum is also the square of the amplitude spectrum. Therefore the zeros in the determininant of the autocorrelation matrix, Φ_{aa}, probably occur for the same reasons that they occur in the amplitude spectrum. The relationship between the instabilities of equations (26) and (28) has not yet been fully investigated.

Fig. 17(a) shows the response, R_s, at a point a long way vertically below a point source of frequency f, which is a distance D below the sea surface. Fig. 17(b) shows the response, R_a, of a point detector, a distance D below the sea surface, to a vertically-travelling plane wave of frequency f. In each case the distance between source and receiver is assumed to be very large compared with D so that spherical divergence can be ignored. Interference occurs between the direct wave and the wave reflected off the sea surface. The response is the same in each case:

$$R = \sin(2\pi ft) + \sin(2\pi f t + 2Df \,.\, 2\pi/c_\infty - \pi).$$

The value of R is zero whenever

$$2Df \,.\, 2\pi/c_\infty - \pi = (2n-1)\,\pi,\ n = 1, 2, \text{etc.} \tag{29}$$

Rewriting equation (29) we have

$$2Df/c_\infty = n,\ n = 1, 2, \text{etc.} \tag{30}$$

Therefore, $D = \frac{1}{2}n\lambda$, $n = 1, 2$, etc., where $\lambda = c_\infty/f$. Therefore, whenever the source depth, H, or detector depth, D, corresponds to a multiple of $\lambda/2$, the amplitude of the Fourier transform, $|PTT(\nu)|$, at the frequency

$$\nu = c_\infty/\lambda$$

will be zero, and the spiking filter calculation will go unstable because the determinant of the autocorrelation matrix of $PTT(t)$ will be small. Since the optimum depths for the gun and the receiver correspond to $\lambda/4$, the amplitude spectrum of the returning wave will contain zeros at even multiples of the bubble oscillation frequency, if the system response has been optimized. If the gun depth, H, and detector depth, D, are different, there will be two sets of zeros in the amplitude spectrum of the returning wave. This result is perfectly general and applies to every marine seismic reflection profiling system which can be considered to have a point source and a point receiver.

In terms of calculating the filter coefficients, f_n, the theoretical signal has to be sampled a discrete intervals. The Fourier transform of the sampled signal is also

Downloaded from http://gji.oxfordjournals.org/ at Edinburgh University on August 26, 2013

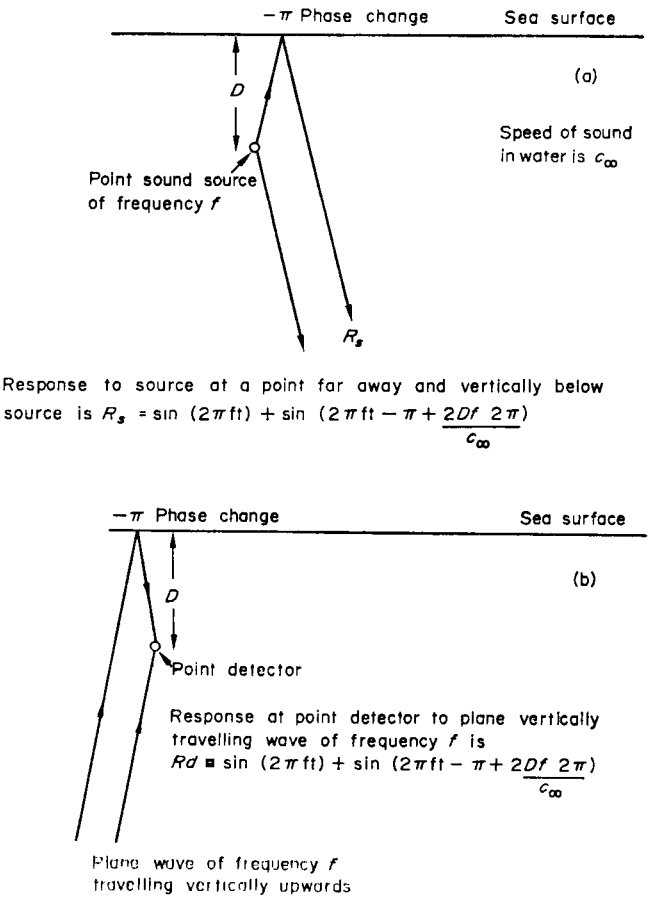


FIG. 17. A diagram to show how the phase reversal at the sea surface affects the response (a) vertically below a source of frequency f and depth D (b) at a point detector for vertically-travelling plane waves of frequency f. Spherical divergence has been neglected.

discrete. It is possible that none of these frequencies is close enough to the frequencies of the continuous Fourier transform at which zeros occur, for the calculation to become unstable. In this case $\det \Phi_{aa}$ in equation (28) will be very small, but not small enough to make the right-hand side of equation (28) too large.

It should be noted that this problem does not occur in the conventional processing technique. The equations which are solved using the approach of Robinson & Treitel (1967) are equations (4)

$$\sum_{n=0}^{M} f_n[\phi_{aa}(0) \cdot \phi_{aa}(n-\tau)+\phi_{vv}(n-\tau)] = \phi_{aa}(0) \cdot \phi_{da}(\tau) \quad \text{for} \quad \tau = 0, 1, \ldots, M. \quad (4)$$

The solution of these equations will be unstable if the discrete Fourier transforms of the information wavelet, a_t, and the noise series, v_t contain zeros at the same frequencies. This, in general, is not the case. The noise usually contains energy at all frequencies.

Let us now return to a consideration of the calculation of a spiking filter for the data of Fig. 20(a). The raw data were sampled at 5 ms intervals, giving a Nyquist

Downloaded from http://gji.oxfordjournals.org/ at Edinburgh University on August 26, 2013

frequency of 100 Hz. If the theoretical wave were sampled at 5 ms intervals and filtered with an anti-alias filter there would be no energy in the Nyquist frequency and so instability in the calculation of the spiking filter would occur. To avoid this instability, due to lack of energy in the high frequencies, some energy is introduced by low-pass filtering the theoretical waveform with a Gaussian filter having a cut-off frequency of 120 Hz. This introduces a certain amount of aliasing. This procedure of introducing a little aliasing was also used in Section 2 of this paper to stabilize another filter.

Fig. 18 shows the theoretical waveform, sampled at 5 ms intervals, and its amplitude spectrum. The theoretical waveform $PTT(t)$ is the theoretical arrival for a perfect reflection at 1200 fathoms. The zeros in the amplitude spectrum of $PTT(t)$ at about 50 Hz and 100 Hz are due to the surface reflection effects already discussed. It can be seen from equation (30) that zeros will occur at frequencies

$$f_s = \frac{n.1500}{2.14}\text{Hz}, \; n = 1, 2, \text{etc.}$$

at the source, and

$$f_d = \frac{n.1500}{2.15}\text{Hz}, \; n = 1, 2, \text{etc.},$$

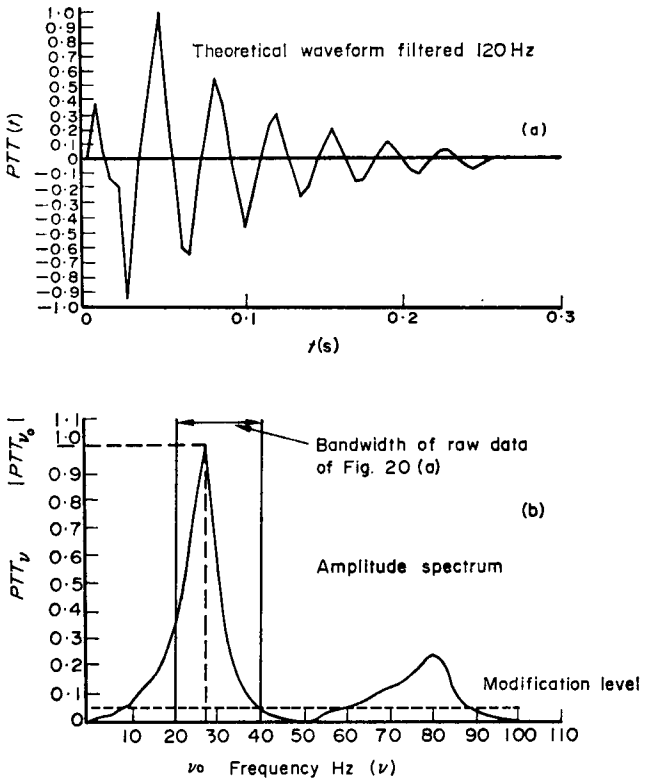


FIG. 18. (a) The theoretical waveform, $PTT(t)$, of Fig. 16 after passing through a low-pass filter with a cutoff of e^{-1} at 120 Hz, and digitizing it at 5 ms intervals. (b) The amplitude spectrum, $|PTT_\nu|$, of (a) which has been normalized so that the maximum value, $|PTT_{\nu_0}|$, is 1·0. The zeros at about 50 Hz and 100 Hz are the result of the phase reversal effects of Fig. 17.

Downloaded from http://gji.oxfordjournals.org/ at Edinburgh University on August 26, 2013

at the detector, where a figure of 1500 ms^{-1} has been used for the speed of sound in water. Since the frequencies at which the amplitude is zero are very close to the two discrete frequencies 50 Hz and 100 Hz in the discrete Fourier transform, PTT_ν, of the theoretical waveform, some modification of the waveform is necessary before a stable filter can be calculated. The modification may be performed using the following technique.

The discrete Fourier transform, PTT_ν, of the theoretical waveform, $PTT(t)$, is examined. It is composed of real, R_ν, and imaginary, I_ν, parts, at each frequency ν. The amplitude at the frequency ν is given by

$$|PTT_\nu| = \sqrt{(R_\nu^2 + I_\nu^2)}.$$

The phase, θ_ν, at frequency ν, is given by

$$\tan\theta_\nu = (I_\nu/R_\nu).$$

If the amplitude of the Fourier transform, $|PTT_\nu|$, at a frequency ν, is less than a certain desired fraction of the maximum amplitude of the transform, $|PTT_{\nu_0}|$, at the dominant frequency, ν_0, then R_ν and I_ν are both multiplied by the same quantity, Q_ν, which will increase $|PTT_\nu|$ to the desired level. This procedure will not alter the phase, θ_ν. After this modification process the modified wavelet, $PTT_m(t)$, is formed by the inverse transform

$$PTT_m(t) = \lim_{N\to\infty} \frac{1}{2N+1} \sum_{\nu=-N}^{N} |PTT_{m\nu}| \exp(i\theta_\nu) \exp[2\pi i\nu t/(2N+1)].$$

The unmodified waveform, $PTT(t)$, was originally real-valued. Since the phase, θ_ν, at frequency ν, is the same for both the modified and unmodified waveforms, the modified waveform, $PTT_m(t)$, is also real-values.

The modification level was varied from 2 to 8 per cent of the maximum amplitude, $|PTT_{\nu_0}|$. From these various waveforms spiking filters were calculated using equations (5)

$$\sum_{n=0}^{M} f_n \phi_{aa}(n-\tau) = \phi_{da}(\tau) \quad \text{for} \quad \tau = 0, 1, 2, \ldots, M$$

where the input wavelet, a_t, was the modified wavelet, $PTT_m(t)$, and the desired output, d_t, was a spike of unit amplitude. The spike position was varied as described in Section 2 of this paper, and the optimum filter, for a desired average squared error of less than 0·1, was found. The optimum filters for the waveforms with 2–8 per cent modification are shown in Fig. 19. Also shown in Fig. 19 are the results of filtering the unmodified 50 Hz waveform of Fig. 16.

Each filter is designed, therefore, to give a spike output for an input wave containing energy up to 100 Hz. The output from each filter shown in Fig. 19 is for an input waveform containing energy only up to 50 Hz. The width of the spike is of the order of the shortest wavelength present in the input to the filter. Consequently, the lower frequency input will produce broadening on both sides of the spike. It is clear from Fig. 19 that the more the input wave is modified, that is, the more energy is injected at about 50 Hz and 100 Hz, the less energy is present at 50 Hz and 100 Hz in the filter. It is clear that instability occurs by severe oscillations at these frequencies, unless some modification is made. The breadth of the spike is not altered as the level of modification is increased, but, for the low-frequency unmodified input, the side-lobes on each side of the spike are increased. This is to be expected: the more the shape of the original waveform is distorted, the less the output, for an undistorted input, will look like the desired output. Of course, since even the unmodified wave is only a good approximation to the real wave, the output for a real arrival will be even less like a clean spike. Therefore it is expected that the best filter which can be

Downloaded from http://gji.oxfordjournals.org/ at Edinburgh University on August 26, 2013

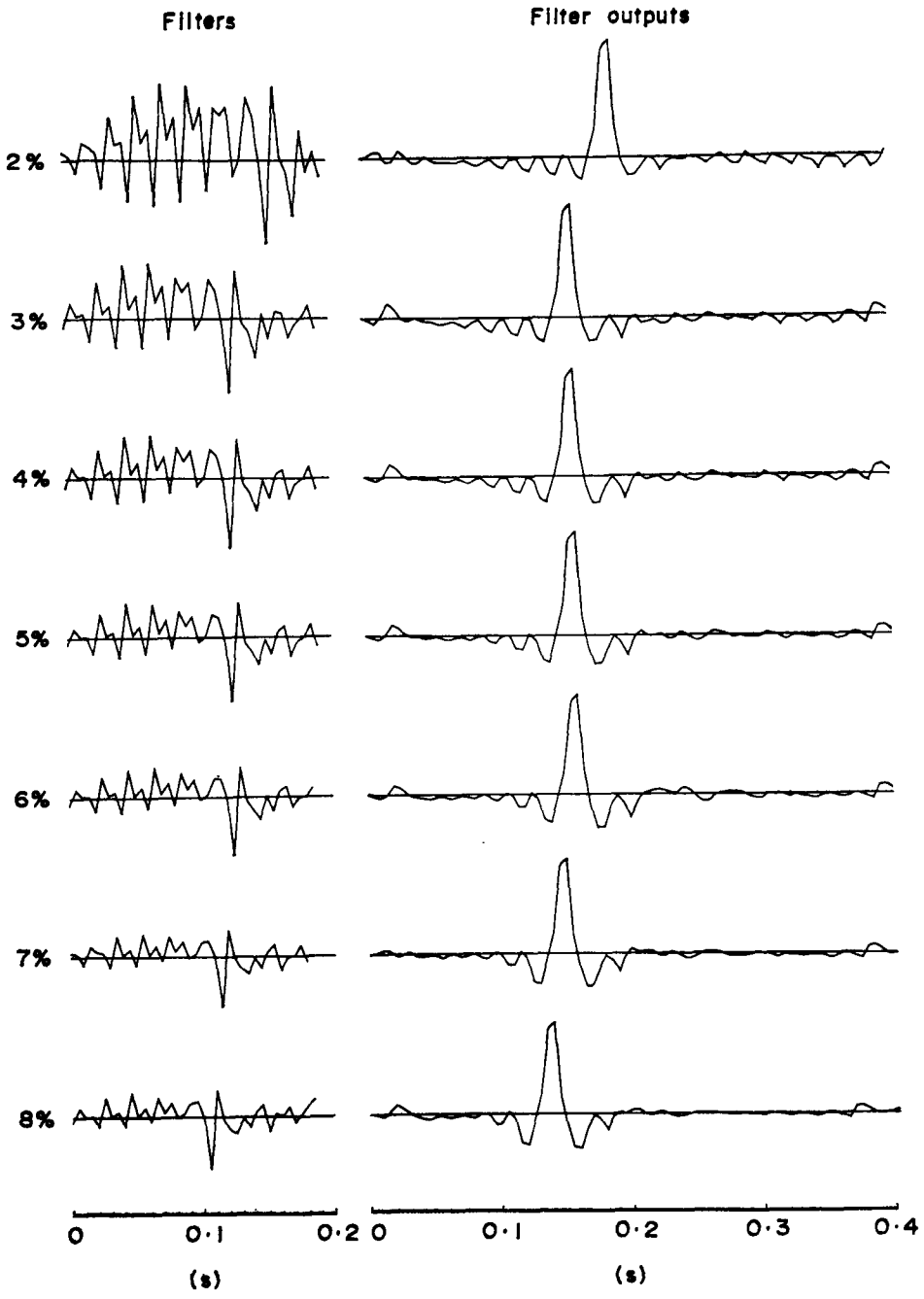


FIG. 19. The filters are calculated from modified versions of *PTT*(*t*) of Fig. 18(a), each modification corresponding to the level below which the modified amplitude spectrum does not drop. The outputs are the result of filtering the last waveform of Fig. 16 with each filter.

Downloaded from http://gji.oxfordjournals.org/ at Edinburgh University on August 26, 2013

achieved is that which is stable and derived from the least modified theoretical waveform.

It should be noted that none of these filters could have been calculated using conventional techniques. The unmodified waveform in Fig. 18(a) can be expressed as a z-transform with 52 coefficients. This z-transform has 51 roots, 17 of which lie inside the unit circle. Thus the waveform is nowhere near being minimum-delay.

The results of filtering the raw data of Fig. 20(a) with the 2 per cent filter and the 5 per cent filter of Fig. 19 are shown in Fig. 20(b) and (c). Both filters produce delays; therefore the traces (b) and (c) of Fig. 20 have been shifted back by the correct delay times to make all arrival times of all three traces line up.

Both filters considerably improve the appearance of the data, but the 5 per cent filter produces sharp negative peaks after each positive peak. The sharp negative peaks are absent in the output of the 2 per cent filter. This is to be expected: the 5 per cent filter is designed to spike a waveform which differs more from the real arrival than does that for which the 2 per cent filter was designed.

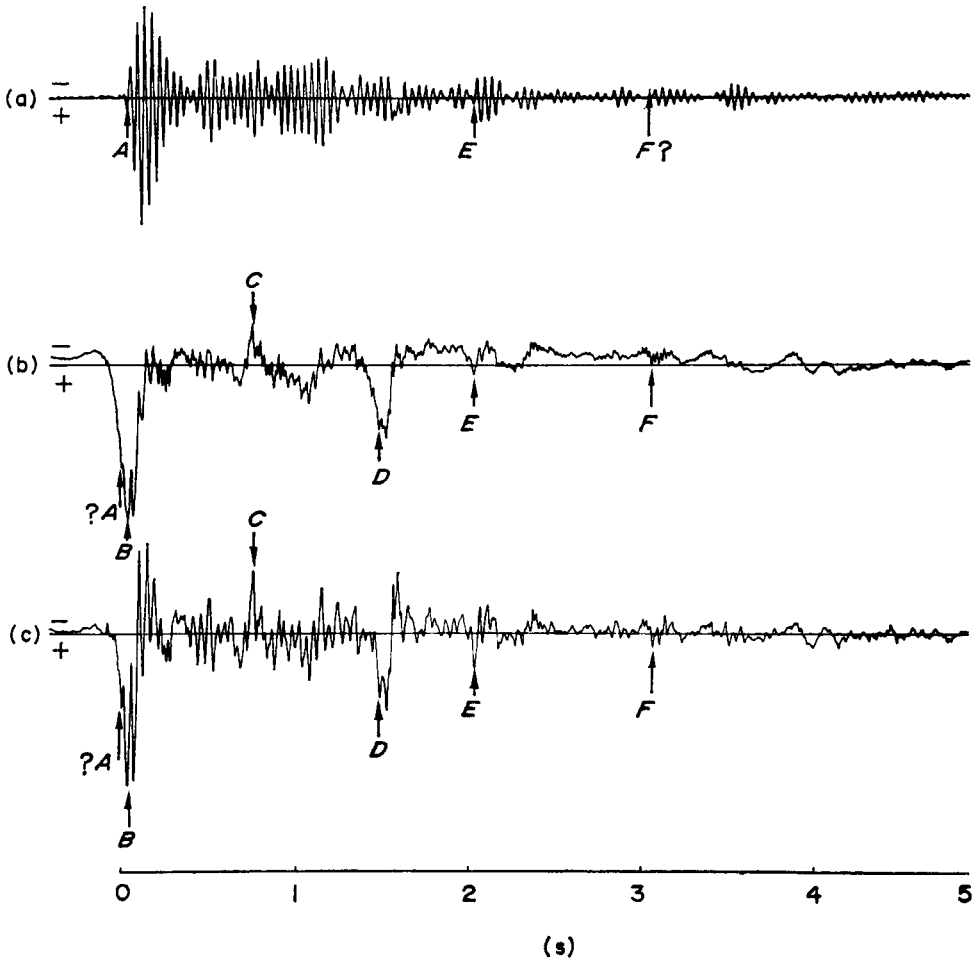


FIG. 20. (a) Raw data trace recorded in the bandwidth 20–40 Hz. (b) Result of filtering (a) with the 2 per cent filter of Fig. 19. (c) Result of filtering trace (a) with the 5 per cent filter of Fig. 19. The filter delays have been removed from (b) and (c) so that the sea bottom arrival at A lines up on all three traces.

Downloaded from http://gji.oxfordjournals.org/ at Edinburgh University on August 26, 2013

Time on all three traces is measured from the sea bottom arrival at A, which can clearly be seen on trace (a), but only very doubtfully on traces (b) and (c), for immediately following this arrival are reflections, B, from two reflectors immediately below the sea floor. It is impossible to resolve these in the raw data trace, a. The arrival C is interpreted as a negative reflection. This occurs as a result of a sudden decrease in acoustic impedance, ρc, where ρ is the density and c the P-wave velocity in the medium. Arrival D is a very strong reflector at about 1·5 s, which can hardly be seen in the raw data. Between B and D there seem to be no striking reflectors apart from the negative one at C. There is probably a gradual change of physical properties of the media in this region. E is an arrival which is clearly seen in all three traces at about 2·1 s. The multiple of the sea floor can be seen coming in again at F after 3·1 s.

The trace 20(a) was obtained in an area of thick sediments south-west of Ireland in the N. Atlantic. The base of the sediments is about 7 km below the sea floor and might be seen as a low-frequency arrival at about 4 s. (Scrutton 1970).

The 2 per cent filter appears to give slightly less resolution than the 5 per cent filter, but there is no evidence that it gives spurious peaks, and is therefore the better filter. It is quite clear that the 2 per cent filter will only produce a spike when an arrival is present: random noise is unaffected by the filter, as is seen on the trace before the sea bottom arrival at A; even signal generated noise, which is probably what exists between 4 and 5 s, is unaffected.

It is concluded that filters of this design will increase the signal to noise ratio, because they have the effect of adding all the energy in an arrival, which previously was spread over a broad time-span, and outputting it all in one burst. The noise does not correlate over the time-space of the filter and is therefore unaffected.

4. Application of the method to the design of a system with more than one air gun

Suppose that it is desired to design a system with the maximum energy return for every reflection, and to compress all this energy into a spike, so that the reflectors can be seen clearly. It will be assumed that a number of guns of different sizes is available. The optimum depth for guns of each size can be determined from Fig. 14, if the operating pressure is approximately known, provided the gun sizes do not exceed 100 cu. in. If the gun sizes do exceed this value it is possible to determine the period of oscillation for every desired set of conditions using the bubble theory (Ziolkowski 1970).

A desired waveform, $PT(t)$, to enter the sea floor can be constructed by calculating a separate waveform for each of the separate gun sizes, and superposing all the waveforms. Delays of the firing instants of the deeper guns relative to the firing instants of the shallower guns may be desirable. The shape of the waveform which enters the sea floor, $PT(t)$, can be calculated in this way with a computer; it is not necessary to spend hours at sea making trial-and-error measurements. With a number of guns at different depths it is possible to eliminate zeros in the amplitude spectrum of $PT(t)$. The only restriction of this method is that the guns be sufficiently far apart for the bubble from each gun to behave independently of the other bubbles.

The depth of the receiver, D, can then be determined such that $PTT(t)$ has maximum energy. $PTT(t)$ is bound to have zeros in the amplitude spectrum of its Fourier transform.

The method may also be applied to existing systems to improve the design of spiking filters. It is unlikely that every arrival, for systems using air guns, is minimum-delay. In this case, when the only available information about the shape of the waveform is its autocorrelation function, the only Wiener filter in use at present which will contract the wavelet, is the Prediction Error Filter (Peacock & Treitel 1968). It is only necessary to have guns far enough apart, and to know the depths and pressure of all the guns, and the depth of the streamer, for the method presented in

Downloaded from http://gji.oxfordjournals.org/ at Edinburgh University on August 26, 2013

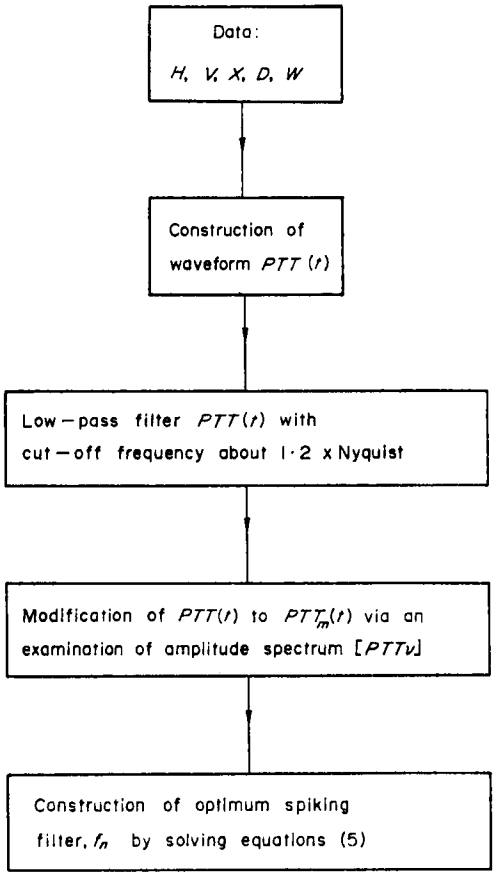


FIG. 21. Steps in the construction of a spiking filter from a set of data. There is one data set for each gun; the construction of the waveform $PTT(t)$ is formed by the superposition of all the individual arrival waves for the separate guns.

this paper to be applied. If there is little variation in the depths and pressure of the guns, one filter will work for every shot. If one gun stops working, the fact can easily be recorded, and a new filter designed if necessary.

A diagram summarizing the various steps in the calculation of the spiking filter is shown in Fig. 21.

Acknowledgments

Most of the ideas presented here are the results of clarifying rather woolly notions in discussions with Dr D. P. McKenzie. Without his help a great deal of this work could not have been attempted. Sir Edward Bullard and Mr A. M. Merzer have both contributed helpful suggestions for theoretical aspects of this work.

All the data presented here were obtained with the help and co-operation of my supervisor Dr F. Gray, and Mr T. R. E. Owen.

Downloaded from http://gji.oxfordjournals.org/ at Edinburgh University on August 26, 2013

References

Bareiss, E. H., 1968. The numerical solution of polynomial equations and resultant procedures. In: *Mathematical Methods for Digital Computers*, eds Ralston, A. and Wilf, H. S., John Wiley, New York.

Berkhout, A. J., 1970. *Minimum Phase in Sampled Signal Theory*, Unpublished Ph.D. Thesis. Koninklijke Shell Exploration and Production Laboratory, Rijswijk, Netherlands.

Copson, E. T., 1970. *An Introduction to the Theory of Functions of a Complex Variable*, Oxford University Press.

Giles, B. F., 1968. Pneumatic acoustic energy source, *Geophys. Prospect.*, **16,** (No. 1), 21–53.

Kirkwood, J. G. & Bethe, H. A., 1942. *OSRD Report*, No. 588.

Knudsen, W. C., 1961. Elimination of secondary pressure pulses in offshore exploration, *Geophysics*, **26,** No. 4, 425–436.

Lavergne, M., 1968. *Emission by underwater explosions*, Institut Francais du Petrole, Ref. 16261.

Levinson, N., 1949. The Wiener R.M.S. error criterion in filter design and prediction. Appendix B of Wiener, N., 1949. *Extrapolation, Interpolation and Smoothing of Stationary Time Series*, Wiley, New York.

Peacock, K. L. & Treitel, S., 1968. Predictive deconvolution: theory and practice, *Geophysics*, **34** (No. 2), 155–169.

Roberts, D. G., Bishop, D. G., Laughton, A. S., Ziolkowski, A. M., Scrutton, R. A. & Matthews, D. H., 1970. New sedimentary basin on Rockall Plateau, *Nature, Lond.*, **225** (5228), 170–172.

Robinson, E. A., 1957. Predictive decomposition of seismic traces, *Geophysics*, **22,** No. 4, 767–778.

Robinson, E. A., 1967. *Statistical Communication and Detection with special reference to Digital Data Processing of Radar and Seismic Signals*, Charles Griffin, London.

Robinson, E. A. & Treitel, S., 1967. Principles of Digital Wiener filtering, *Geophys. Prospect.*, **15** (No. 3), 311–333.

Scrutton, R. A., 1970. Personal Communication, Department of Geodesy and Geophysics, Madingley Rise, Cambridge.

Treitel, S. & Robinson, E. A., 1966a. Seismic wave propagation in layered media in terms of communication theory, *Geophysics*, **31** (No. 1), 17–32.

Treitel, S. & Robinson, E. A., 1966b. The design of high-resolution digital filters. *I.E.E.E. Trans. GE*-4, **No. 1**, 25–38.

Wiener, N., 1949. *Extrapolation, Interpretation and Smoothing of Stationary Time Series*, Wiley, New York.

Ziolkowski, A., 1970. A method for calculating the output pressure waveform from an air gun, *Geophys. J. R. astr. Soc.*, **21,** 137–161.

Note added in proof

Sometimes a_t is defined to be minimum-delay only if $|z_i| > 1$, for only then does it have a realizable inverse. But if the definition is to be consistent with the frequency-domain definition of minimum phase-lag, for a given power spectrum, then the $\geqslant$ sign applies.

Appendix

Separation of the information wavelet autocorrelation function from the noise autocorrelation function

The seismic signal, x_t, is composed of signal u_t, and noise, v_t. It was shown in Section 1 that the signal, u_t, can be thought of as a source wavelet or information

Downloaded from http://gji.oxfordjournals.org/ at Edinburgh University on August 26, 2013

wavelet, a_t, which has been convolved with the ideal impulse response of the layered earth, α_t. Thus

$$x_t = \alpha_t * a_t + v_t.$$

Robinson & Treitel (1967) show how this information allows the autocorrelation function, $\phi_{xx}(\tau)$, of the seismic trace, x_t, to be expressed as

$$\phi_{xx}(\tau) = \phi_{aa}(0) \cdot \phi_{aa}(\tau) + \phi_{vv}(\tau) \tag{A1}$$

provided u_t and v_t are uncorrelated.

If an adjacent trace, x_t^1, recorded over the same geology, with the same impulse response, α_t, is considered, it will have different noise from the first trace. The composition of this adjacent trace can thus be written

$$x_t^1 = \alpha_t * a_t + v_t^1.$$

It has been assumed that the information wavelet, a_t, is the same in each case. The cross-correlation function of the two traces is

$$\begin{aligned}\phi_{xx'}(\tau) &= \sum_{t=-\infty}^{\infty} x_{t+\tau} x_t^1 \\ &= \sum_{t=-\infty}^{\infty} (\alpha_{t+\tau} * a_{t+\tau} + v_{t+\tau})(\alpha_t * a_t + v_t^1) \\ &= \phi_{aa}(0) \cdot \phi_{aa}(\tau). \end{aligned} \tag{A2}$$

In the last step it has been assumed that $\phi_{aa}(\tau) = 0$ for all $\tau \neq 0$ and that v_t, v_t^1, u_t are uncorrelated. Therefore $\phi_{aa}(0) \cdot \phi_{aa}(\tau)$ can be obtained from equation (A2) and $\phi_{vv}(\tau)$ can be obtained by subtraction of equation (A2) from equation (A1).

Downloaded from http://gji.oxfordjournals.org/ at Edinburgh University on August 26, 2013